the plant journal

SEB SOCIETY FOR EXPERIMENTAL BIOLOGY

The Plant Journal (2021) doi: 10.1111/tpj.15391

Pericentromeric chromatin reorganisation follows the initiation of recombination and coincides with early events of synapsis in cereals

Andrea Lenykó-Thegze[1], Attila Fábián[1], Edit Mihók[1], Diána Makai[1], András Cseh[2]* and Adél Sepsi[1,3]*

[1]*Department of Biological Resources, Eötvös Loránd Research Network, Centre for Agricultural Research, Brunszvik u. 2, Martonvásár 2462, Hungary,*

[2]*Department of Molecular Breeding, Eötvös Loránd Research Network, Centre for Agricultural Research, Brunszvik u. 2, Martonvásár 2462, Hungary, and*

[3]*Department of Applied Biotechnology and Food Science (ABÉT), BME, Budapest University of Technology and Economics, Műegyetem rkp. 3-9, Budapest 1111, Hungary*

Received 16 March 2021; revised 4 June 2021; accepted 14 June 2021.

*For correspondence (e-mail: sepsi.adel@atk.hu; cseh.andras@atk.hu).

[Correction added on 06 August 2021, after first online publication: The email address of András Cseh has been updated in this version.]

SUMMARY

The reciprocal exchange of genetic information between homologous chromosomes during meiotic recombination is essential to secure balanced chromosome segregation and to promote genetic diversity. The chromosomal position and frequency of reciprocal genetic exchange shapes the efficiency of breeding programmes and influences crop improvement under a changing climate. In large genome cereals, such as wheat and barley, crossovers are consistently restricted to subtelomeric chromosomal regions, thus preventing favourable allele combinations being formed within a considerable proportion of the genome, including interstitial and pericentromeric chromatin. Understanding the key elements driving crossover designation is therefore essential to broaden the regions available for crossovers. Here, we followed early meiotic chromatin dynamism in cereals through the visualisation of a homologous barley chromosome arm pair stably transferred into the wheat genetic background. By capturing the dynamics of a single chromosome arm at the same time as detecting the undergoing events of meiotic recombination and synapsis, we showed that subtelomeric chromatin of homologues synchronously transitions to an open chromatin structure during recombination initiation. By contrast, pericentromeric and interstitial regions preserved their closed chromatin organisation and become unpackaged only later, concomitant with initiation of recombinatorial repair and the initial assembly of the synaptonemal complex. Our results raise the possibility that the closed pericentromeric chromatin structure in cereals may influence the fate decision during recombination initiation, as well as the spatial development of synapsis, and may also explain the suppression of crossover events in the proximity of the centromeres.

Keywords: *Triticum aestivum*, *Hordeum vulgare*, meiosis, meiotic recombination, centromeric crossovers, chromatin dynamism, chromatin packaging, synaptonemal complex.

INTRODUCTION

Chromosomes in the cell nucleus are composed of arrays of chromatin loops irregularly folded into three-dimensional chromosome domains that are framed by prominent structural features called centromeres and telomeres (Heslop-Harrison and Schwarzacher, 2011; Jerković et al., 2020). The spatial organisation of chromosomes is defined by the extent of this chromatin folding, which has a major impact on key biological processes, such as DNA replication, recombination and transcription (Bell et al., 2011; Jordan et al., 2020). The capacity to quickly alter chromatin structure during the mitotic and meiotic cell cycle provides a considerable plasticity to chromosomes and allows implementation of a multitude of functions (Ma et al., 2015; Pecinka et al., 2020; Tiang et al., 2012). One fundamental developmental programme requiring abrupt adjustments in chromosome architecture is prophase I of meiosis (Loidl, 2016; Ronceret and Pawlowski, 2010; Schwarzacher, 2003). At the heart of prophase I lies the process of meiotic recombination, which

involves the exchange of genetic material between one of the two chromatids of the homologous chromosomes, resulting in a wide variety of genetic diversity within the gametes. Besides ensuring genetic exchange, recombination provides physical connections between the homologous chromosomes, a fundamental requirement for accurate chromosome segregation. Meiotic recombination begins with the formation of programmed DNA double-strand breaks (DSBs) (Keeney et al., 1997) followed by 5′- to 3′ DNA end resection, homology search and strand invasion into an intact, homologous double stranded DNA segment located on one of the chromatids of the homologous partner chromosome (Hunter and Kleckner, 2001; Pradillo et al., 2012). The number of DSBs exceeds 700 per meiosis in hexaploid wheat (*Triticum aestivum*) and only a minority (typically one per chromosome arm) of them result in crossovers (Gardiner et al., 2019), whereas the majority are processed via repair mechanisms resulting in non-crossovers.

The introduction of genome-wide DSBs coincides with the progressive loading of proteinaceous axial elements along the chromosome axes (Armstrong et al., 2002; Chambon et al., 2018). Following homology recognition and strand invasion, the biochemical process of recombination becomes stabilised by the establishment of the synaptonemal complex (SC) (Higgins et al., 2005; Osman et al., 2006), which builds up between the homologous chromosomes in a meiosis-specific process termed synapsis. The SC is formed progressively by connecting axial elements (now becoming lateral elements) of the homologues via transverse filament proteins, which gives rise to the central element of the SC (Zhang et al., 2014). In many organisms, including higher plants, homologous recombination relies on the SC (Barakate et al., 2014) and crossover maturation occurs when homologues attain perfect synapsis.

These critical DNA- and synaptic events are spatially restricted along the chromosomes, so that mature crossover distribution (cytologically manifested as chiasmata within metaphase I chromosomes) recombination- and synapsis initiations occur in the euchromatic subtelomeric regions (Higgins et al., 2012; Osman et al., 2021). Chromosomes in the meiotic nucleus are spatially polarised themselves by telomere and centromere associations formed at the two extremes of the nucleus (Bass et al., 1997; Murphy et al., 2014; Naranjo and Corredor, 2004; Phillips et al., 2012). In this configuration, each chromosome forms a large loop with the ends (telomeres) attached to the nuclear envelope and folded back at the centromere at the opposite side of the nucleus. Immediately preceding synapsis initiation, a transient nuclear arrangement, the telomere bouquet, is almost universally formed inside the pollen mother cell nuclei (Scherthan, 2001) where telomeres are gathered together in a single group (Bass, 2003) and associate with the nuclear envelope (Varas et al., 2015). The telomeres assembled in the bouquet lead mechanical forces from the cytoskeleton to the chromosomes initiating the rapid movement characteristic of prophase I (Sheehan and Pawlowski, 2009; Sepsi and Schwarzacher, 2020). Rapid chromosome movements represent one of the most important elements of homology search because they can facilitate both chromosome encounters and dissociations (Chacón et al., 2016; Martinez-Garcia et al., 2018). Together with other prominent features of chromatin dynamics, prophase movements of chromosomes outline a strong mechanical aspect of meiosis that appears to be crucial for the initiation of meiotic recombination, homology recognition and progression of DSB repair pathways (Zickler and Kleckner, 2015). During the period of telomere bouquet formation, a highly dynamic chromatin reorganisation became clear from *in situ* hybridisation studies performed on nuclei of wheat and wheat-rye introgression lines (Colas et al., 2008; Corredor et al., 2007; Maestra et al., 2002; Prieto et al., 2004; Schwarzacher, 1997). An extreme polarisation of the meiotic nuclei was shown by the formation of the large centromere groups close to the nuclear envelope (Martinez-Perez et al., 2003) that led to the massive reorganisation of the centromeric chromatin. This implied the transition of the centromeric chromatin from a compact conformation to elongated structures, which coincided with the resolution of the centromeres from the groups and the nuclear periphery (Martinez-Perez et al., 2003). A pre-bouquet conformational change has also been shown for the subtelomeric regions (Prieto et al., 2004) and this phenomenon has subsequently became linked to homology recognition and pairing (Colas et al., 2008). Recent progress in describing the key modulators of plant meiosis (Mercier et al., 2015) allows the application of protein antibodies as meiotic markers to provide the accurate meiotic timing for chromatin dynamics studies supporting an integrated understanding of the complex multifaceted process of meiotic prophase I (Colas et al., 2017; Hurel et al., 2018; Osman et al., 2018; Sepsi et al., 2017; Varas et al., 2015). For example, centromere clustering and subsequent resolution has been confirmed by immunolabelling active centromeres in wheat and was shown to coincide with specific steps of synapsis (Sepsi et al., 2017). However, how chromatin remodelling at the subtelomeres and chromatin packaging along chromosome arms can be correlated with synapsis progression and the process of DNA recombination remains to be clarified.

Wheat-alien hybrid lines, carrying Robertsonian translocations from a related species added to the wheat background, are generally very stable (Türkösi et al., 2018) and suitable for following chromosome behaviour during the mitotic or meiotic cell cycle. By combining molecular cytogenetics with immunohistochemistry, the alien chromosome segment can be visualised within the accurate

timeline of meiosis and valuable information can be gained about chromosome behaviour during homologous recognition, recombination and synapsis in cereals.

In the present study, we used a 7BS.7HL wheat-barley recombinant chromosome line in which we substituted one pair of wheat chromosome arms to a pair of an entire barley chromosome arms, giving rise to a homologous pair of translocation chromosomes (40 wheat + one pair of wheat-barley translocation chromosome). We followed the chromatin organisation of the two homologous barley chromosome arms as parts of entire chromosomes inside the wheat nucleus from chromosome axis formation to full synapsis. Chromatin organisation of the homologous chromosome arms was investigated by *in situ* hybridisation, as detected by optical sectioning with high-resolution laser scanning confocal microscopy, whereas precise meiotic timing including SC formation and recombination initiation was assessed by immunohistochemistry. Our study showed a temporal difference between the meiosis-specific reorganisation of different chromosomal regions, which correlated with recombination initiation and SC formation. We showed that, during recombination initiation, homologous subtelomeric regions become synchronously remodelled to an open chromatin structure, coincident with chromosome axis formation. During this period, interstitial regions and pericentromeres preserved a closed, highly condensed conformation. Synapsis emerged from the decondensed subtelomeres arranged into the bouquet coincident with the initiation of recombination repair and remodelling of the pericentromeric regions. Late remodelling of the pericentromeres was in line with a delayed juxtaposition between the homologous pericentromeric regions compared to the subtelomeres. Our study points to a clear temporal correlation between chromatin remodelling and key meiotic processes such as recombination repair, chromosome juxtaposition and synapsis. We propose that delayed chromatin remodelling within the pericentromeres has an effect on the fate of recombination repair, such that the closed chromatin structure possibly delays the repair processes, thus lengthening the timeframe for crossover-repair decisions.

RESULTS

Development and cytological characterisation of the wheat-barley translocation line

To investigate the order of chromosome arm pairing during meiotic prophase I in large genome cereals, we developed a wheat-barley translocation chromosome line that carries 20 pairs of normal wheat chromosomes and one pair of wheat-barley translocation chromosomes. The line was obtained by crossing a wheat/barley 7H addition line (21 wheat chromosome pairs and one added pair of barley 7H chromosome) (Molnár-Láng et al., 2012) with Chinese Spring wheat carrying the *ph1b* mutation. The wheat *ph1b* mutation (Griffiths et al., 2006) promotes non-homologous recombination at meiosis (see Experimental procedures) and is thus suitable for inducing intergenomic rearrangements between the wheat and barley chromosomes. We detected the translocation chromosome in the F_2 generation of the cross as a monosome (40 wheat chromosomes and a single translocation chromosome), whereas stable disomics (40 wheat chromosomes and a pair of the translocation chromosomes) (Figure 1a,b) were selected from the F_3 generation. Genomic *in situ* hybridisation showed that the translocation is made up of a wheat chromosome arm fused by its centromere to a complete barley (7H) chromosome arm framed by the barley centromere and a telomere (centric fusion) (Figure 1a). The elimination of the *ph* mutation was confirmed by molecular marker analysis (Xpsr574) showing that the translocation line carries the wild-type *Ph1* allele (Figure S1).

Three-colour fluorescence *in situ* hybridisation (FISH) (with Afa-family, pSc119.2, and pTa71 repetitive DNA probes) allowed identification of all wheat chromosomes present and revealed that the barley chromosome arm translocated to the short arm of wheat chromosome 7B-(7BS) (Figure 1a,b). Barley 7HS and 7HL chromosome arm-specific molecular markers (Bmac0031 SSR and HvCSIF6 STS markers, respectively) (Cseh et al., 2011) identified the barley chromosome arm as 7HL (Figure 1e). These results showed that the translocation occurred between the wheat 7BS and barley 7HL chromosome arms giving rise to the 7BS/7HL translocation. Genomic *in situ* hybridisation (GISH) combined with *in situ* hybridisation of the centromeric retrotransposon of wheat (CRW) and the barley centromere-specific G + C repeat revealed that the centromere of the translocation chromosome carries a hybrid centromere, where one half originates from wheat (7BS centromere) and the other half originates from barley (7HL centromere) (Figure 1c,d). The translocation line showed full fertility (Figure 1f) and exhibited stable chromosome inheritance throughout meiosis II (Figure 2). Consequently, 100% of the screened progenies carried the translocation chromosome pair in the background of 40 wheat chromosomes, indicating that the chromosome set including the barley chromosome arm follows balanced segregation, making the line suitable for studying the behaviour of a chromosome arm during meiotic division of wheat.

SC development and centromere dynamics in the 7BS.7HL translocation line

To study chromosome arm dynamics within an exact meiotic timing in the 7BS.7HL translocation line, key events of synapsis and recombination were visualised by immunolabelling. In wheat and barley, meiocytes within the three anthers per floret are in synchronised meiotic stages and can therefore be regarded as identical with respect to

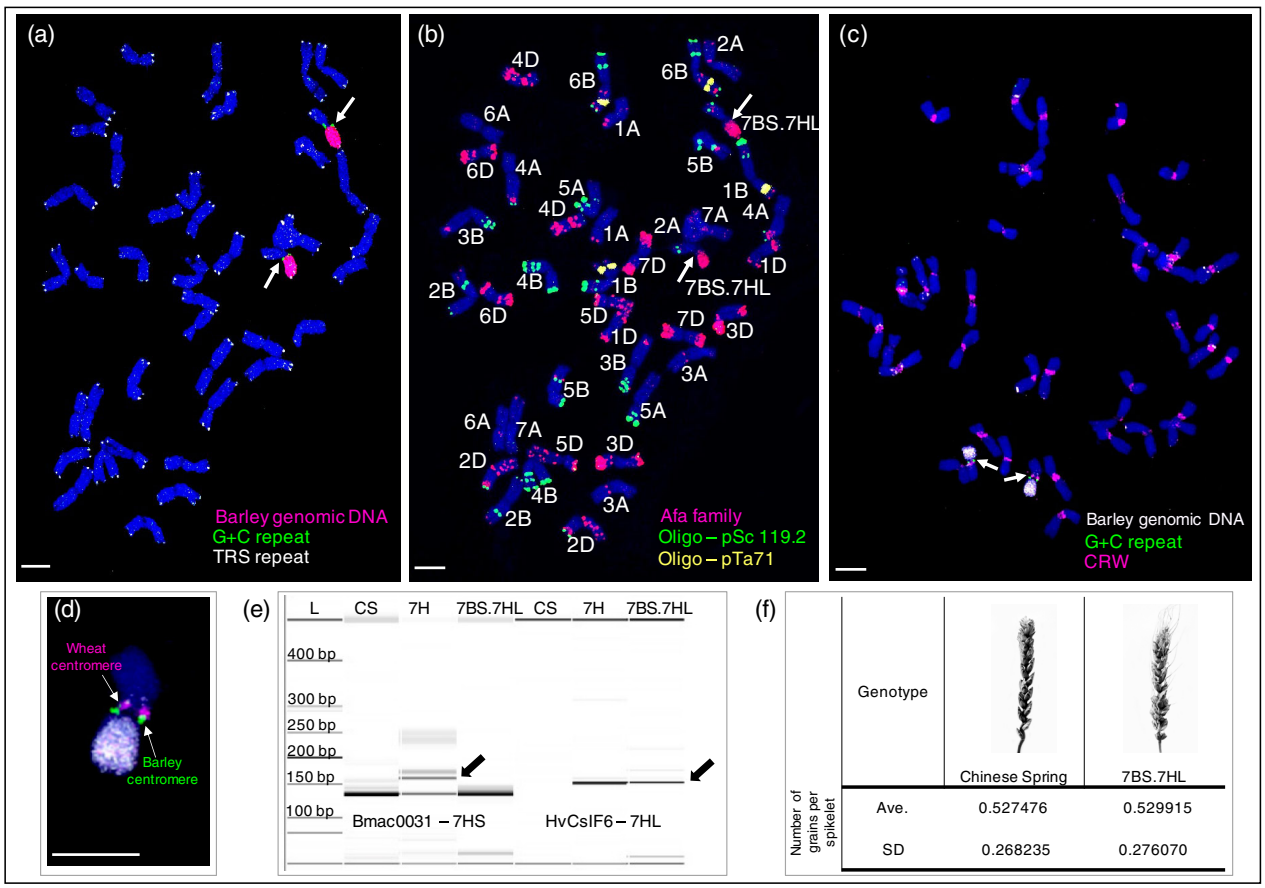

Figure 1. Chromosome composition and fertility of the 7BS.7HL wheat-barley translocation line.
(a) Detection of the translocated 7HL barley chromosome arm together with its centromere and telomere by multicolour *in situ* hybridization on mitotic chromosomes of the 7BS.7HL Robertsonian translocation line. The 7HL barley chromosome arm was labelled with Alexa Fluor 594 (red), the barley centromere-specific G + C repeat sequences (arrow) were detected by Alexa Fluor 488 (green), and all telomeres are shown by the plant telomere-specific repeat sequence (TRS) labelled with Alexa Fluor 647 (far-red and pseudo coloured in grey).
(b) Fluorescence *in situ* hybridization on mitotic chromosomes of the 7BS.7HL Robertsonian translocation line. Repetitive DNA probes Afa family (red), Oligo-pSc119.2 (green) and Oligo-pTa71 (far-red, pseudo coloured in yellow) were used to identify all wheat chromosomes present in the 7BS.7HL translocation line. The translocation chromosome is marked by an arrow and the chromosomes were counterstained with DAPI (blue). Scale bars = 5 μm.
(c) Centromere organisation of the translocation chromosome carrying both barley- and wheat specific centromeric sequences (arrow) as shown by multicolour *in situ* hybridization on mitotic chromosomes of the 7BS.7HL Robertsonian translocation line. *In situ* hybridization visualised the 7HL barley chromosome arm (labelled with Alexa Fluor 647, far-red, pseudo coloured in white), the barley centromere-specific G + C repeat sequences (Alexa Fluor 488, green) and the Ty3/gypsy centromeric retrotransposons of wheat (CRWs) (Alexa Fluor 594, red, pseudo coloured in magenta). DAPI staining is shown in blue. Scale bars = 5 μm.
(d) Close up image of the 7BS.7HL translocation chromosome shown in Figure 1c highlighting the wheat and barley centromeric regions. Scale bars = 5 μm.
(e) Capillary gel electrophoresis patterns of the Bmac0031 (7HS) and HvCslF6 (7HL) barley 7H chromosome arm-specific molecular markers on DNA templates 'Chinese Spring' (CS) wheat, 'Asakazekomugi'/'Manas' 7H disomic addition line (7H) and 7BS.7HL disomic Robertsonian translocation line (RobT). Chromosome arm-specific bands are indicated by arrows.
(f) Spike morphology and fertility of the 7BS.7HL RobT line compared to the parental Chinese Spring wheat. A *t*-test of independence revealed no difference between the fertility potentials of the two genotypes (MD = 0.0024; d.f. = 145, $P = 0.957$). The assumption of homogeneity of variances was tested and satisfied via Levene's *F*-test ($F = 0.009$, $P = 0.924$).

meiotic development (Bennett et al., 1971, 1973a; Schwarzacher, 1997). Meiotic proteins related to the SC axial elements (ASY1) (Armstrong et al., 2002; Boden et al., 2009) and transverse filament proteins (ZYP1) (Higgins et al., 2005) were immunolabelled on preparations made from anthers adjacent to those used to investigate chromosome morphogenesis via *in situ* hybridisation. In addition to SC proteins, active centromeres were labelled concurrently by an anti-centromere-specific histone H3 (anti-CENH3) antibody to confirm the meiotic stages. ASY1 and ZYP1 antibodies revealed the status of the SC progression, whereas CENH3 staining added meiosis-specific centromere dynamics and thus allowed precise measurement of the timing of prophase I. SC formation and centromere dynamics in the 7BS.7HL line proceeded as in wild-type wheat (Desjardins et al., 2020; Osman et al., 2021; Sepsi et al., 2017). Briefly, axial elements formed short stretches along the 4′-6-diamino-2-phenylindole (DAPI) stained

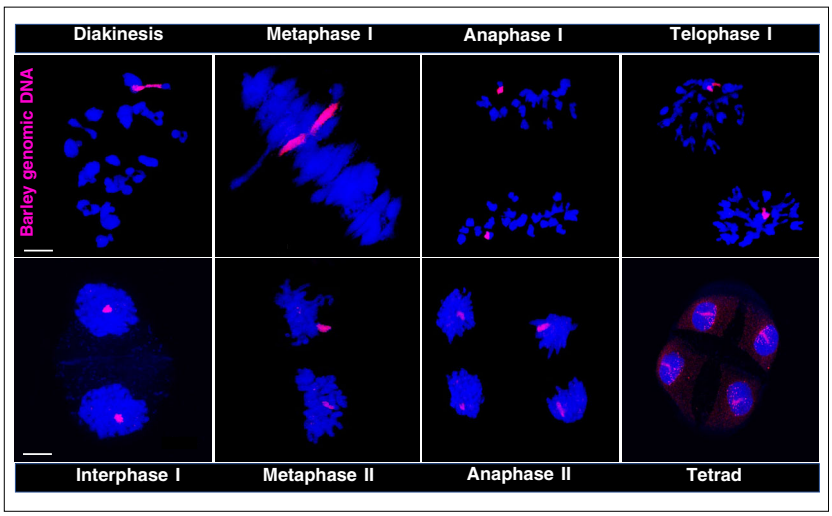

Figure 2. Meiotic segregation of the barley 7HL chromosome arm in the 7BS.7HL wheat/barley disomic translocation line as detected by GISH. The barley genomic DNA probe was labelled with Alexa Fluor 594 (red), whereas the DNA was counterstained with DAPI (blue). The meiotic stages shown are: diakinesis, metaphase I, anaphase I, telophase I, interphase I, metaphase II, anaphase II and tetrad. Scale bar = 5 μm.

chromatin and centromeres associated at one half of the nuclear periphery at early leptotene (Figure 3a). Axial elements were fully linear at late leptotene (Figure S2), whereas the associations of telomeres into the bouquet (telomere bouquet) could be distinguished by the prominent concentration of axial elements at the nuclear periphery, opposite the centromeric pole (Figure 3a). Chromosome synapsis was detected in early zygotene as short stretches of SC central elements opposite the centromere side (Figure S2). Centromeres begin to disperse from the periphery coincident with the appearance of synapsis and later occupied random locations in the nucleus. To be able to provide a detailed reference for chromosome arm pairing as synapsis progressed gradually from early to late zygotene, we subdivided zygotene into four substages according to the extent of the synapsis progression observed within the nucleus. 'Early zygotene' was defined by < 10% of synapsed chromosome axes; 'early-mid zygotene' nuclei were distinguished by 10–50% of synapsed axes where significant subtelomeric synapsis was observed with multiple synapsis initiation events located within the chromosome arms; 'mid zygotene' carried 50–80% synapsed axes and was characterised by progression of chromosome arm synapsis; and 'late zygotene' was defined by 80–95% synapsed axes (Figures 3a and S2). Chromosomes were fully synapsed by pachytene.

Presynaptic chromatin reorganisation: pericentromeric reorganisation is delayed

Having established the stages of SC development in the 7BS.7HL line, we followed the morphogenesis and pairing of the translocated 7HL barley chromosome arm by *in situ* hybridisation on anthers adjacent and thus synchronous (Bennett et al., 1973b) to those accurately staged by ASY1/ZYP1/CENH3 immunolabelling. To reveal the barley chromosome arm and its orientation inside the nucleus, we used a set of different fluorochromes in multicolour FISH experiments and marked barley DNA together with the barley centromere (G + C microsatellite repeat probe) and telomeres (universal telomeric repeat probe). The organisation of the barley chromosome arm was visualised from meiotic initiation through SC formation to the appearance of chiasmata showing mature crossovers between the homologous chromosomes.

Multicolour FISH showed that the 7HL chromosome arms lie parallel in separate territories at early leptotene with the centromeres and telomeres anchored at opposite poles of the nucleus (Figure 3a). The detected barley chromatin was packaged into large globular subdomains at this stage, indicating a closed chromatin structure where the total length of the 7HL barley chromosome arm reached 21.3 ± 7.47 μm (mean ± SD; n = 28) (Figure 3b,c). The distance between the two homologous centromeric or telomeric loci was > 0.2 μm (centromeres and telomeres were perceived as two separate spots) in all cases (n = 71) (Figure 3d), indicating that no centromere- or telomere pairing occurs during leptotene.

In late leptotene nuclei, the telomere bouquet becomes apparent from the accumulation of the telomeric FISH signals in one narrow group at the nuclear periphery (Figure 3a). Concurrently, one part of the barley chromatin, emerging from the telomere bouquet and progressing into the subtelomeres of the 7HL arm, become elongated (chromosome width: 0.22–0.45 μm), indicating the decondensation of the 7HL subtelomeric region (Figure 3a–c). Proximally to this, decondensed subtelomeric

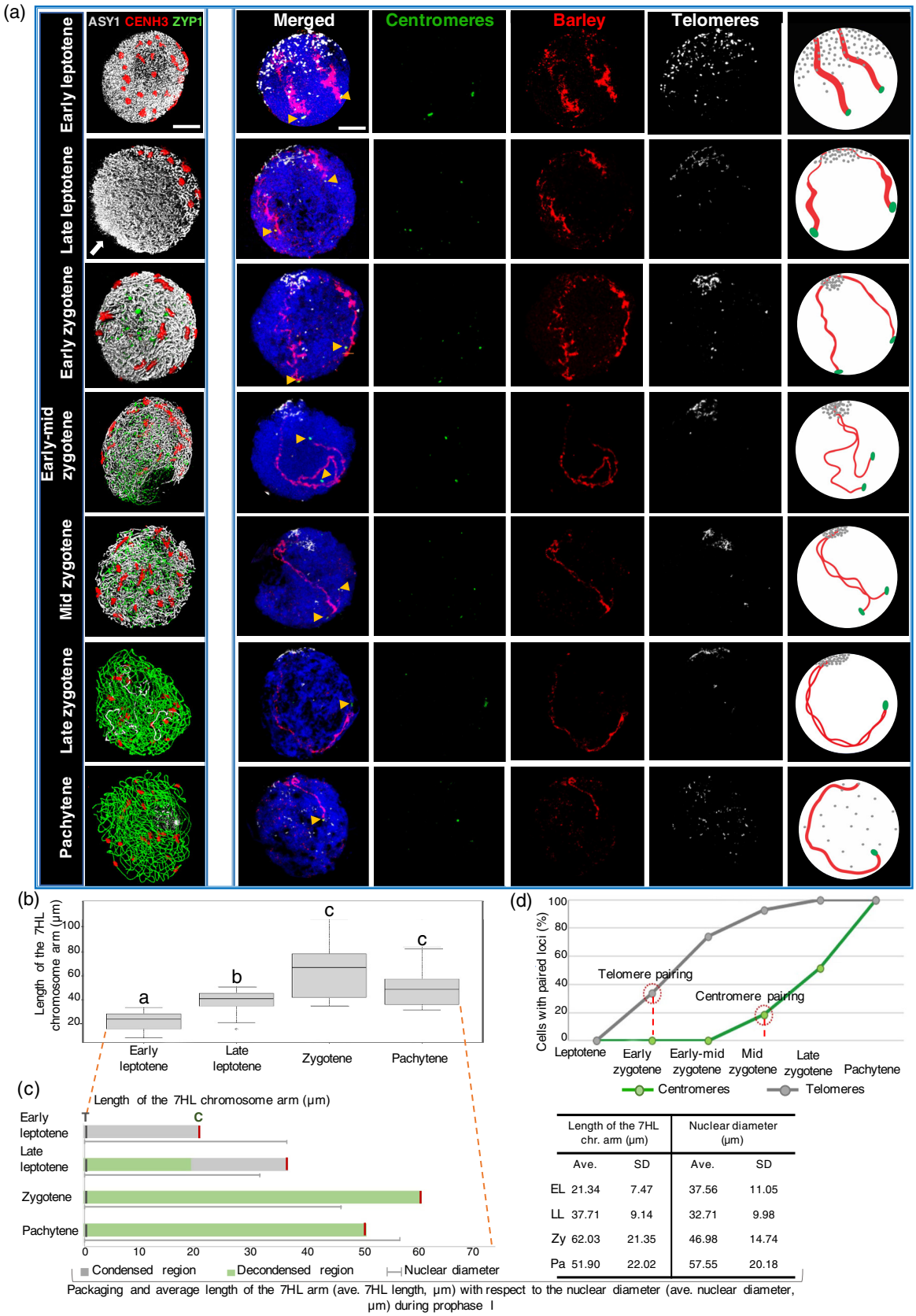

	Length of the 7HL chr. arm (µm)		Nuclear diameter (µm)	
	Ave.	SD	Ave.	SD
EL	21.34	7.47	37.56	11.05
LL	37.71	9.14	32.71	9.98
Zy	62.03	21.35	46.98	14.74
Pa	51.90	22.02	57.55	20.18

Packaging and average length of the 7HL arm (ave. 7HL length, µm) with respect to the nuclear diameter (ave. nuclear diameter, µm) during prophase I

Figure 3. Chromosome arm morphogenesis and pairing of different chromosomal regions during key events of synapsis at meiotic prophase I.
(a) Left: Examples of 7BS.7HL translocation line nuclei at different substages (leptotene to pachytene) of meiotic prophase I, showing synaptonemal complex progression and centromere dynamics. All active centromeres are visualized by an anti-CENH3 antibody (rabbit, detected by Alexa 594, red). The synaptonemal complex axial elements related protein ASY1 and the synaptonemal complex transverse filament protein visualized by anti-ASY1 (guineapig, detected by Alexa 647, pseudo coloured in grey) and rat anti-ZYP1 antibodies (detected by Alexa 488, green) reveal distinct stages of synaptonemal complex development. Formation of the telomere bouquet is seen by intensive ASY1 staining (arrow on the late leptotene image). For single channel images, see Figure S2. Scale bar = 5 μm. Right: *In situ* hybridization showing the orientation and morphogenesis of the homologous barley chromosome arms (red), framed by their centromere (green) and telomere (grey) during substages of meiotic prophase I. Nuclei encompassing meiotic stages from leptotene to pachytene were obtained from adjacent anthers and are thus synchronous to those used for the CENH3, ASY1, ZYP1 immunolabelling (left) (Bennett et al., 1973b). Meiotic nuclei were counterstained with DAPI. Scale bars 5 μm. Early leptotene: Telomeres are dispersed within one half of the nucleus and centromeres are located within the other nuclear hemisphere. The barley chromosome arms are separated and the chromatin is condensed into globular domains. Late leptotene: The telomere bouquet is formed and the barley telomeres although located in close proximity to one another remain separated. The barley centromeres are separated from one another and located close to the nuclear periphery opposite the telomeres. The pericentromeric and interstitial regions maintain their condensed organisation, whereas the subtelomeric regions are elongated into thin chromatin threads. Early zygotene: Barley telomeres are paired, whereas centromeres (green, highlighted by yellow arrowheads) are at the opposite pole of the nucleus and remain separated from one another. The barley chromosome arms running parallel show an elongated organisation that eventually forms finger-like structures curved out transversally on both sides of the chromosome axis. Early-mid zygotene: Close juxtaposition of the barley 7HL from the subtelomeric region onwards demonstrates synapsis initiation while centromeres and the pericentromeric regions remain separated at a considerable distance from each other. Mid zygotene: Subtelomeres colocalise and interstitial regions show numerous 'juxtaposed interstitial segments' with variable length, where the two homologous chromosome arms colocalise. Homologous contacts formed by the 'juxtaposed interstitial segments' are interspersed with non-colocalised, parallel 'interstitial chromatin alignments' of various lengths (for more detail, see Figure 3) and this chromosome configuration extends from the subtelomeres to the pericentromeric regions. Pericentromeres are widely separated from their homologous chromosome segments forming a fork-like structure. Late zygotene: The telomere bouquet disperses; the elongated chromosome arms show multiple 'juxtaposed interstitial segments' disrupted by 'interstitial chromatin alignments' and this conformation reaches the centromeric regions. Centromeres are juxtaposed on the majority of nuclei. Pachytene: Synapsis is fully formed between the homologous barley chromosome arms.
(b) Expansion and condensation of the 7HL chromosome arm during substages of meiotic prophase I Statistical analysis revealed a highly significant difference ($F = 32.614$; d.f. 1 = 3; d.f. 2 = 96; $P = 1.24 \times 10^{-14}$ between the chromosome arm length measured at the different stages. Tukey's B *post hoc* test categorized these differences into three (a, b, c) groups (indicated by lowercase letters): Early Leptotene, Average (ave.): 21.34 (a – shortest); Late Leptotene, Average: 37.58 (b – medium length); Zygotene, Average: 62.03; and Pachytene, Average: 51.90 (both c – longest).
(c) Proportions of the condensed (grey horizontal bar) and decondensed (green horizontal bar) chromosomal regions within the barley chromosome arms (chr. arm) during prophase I with respect to the nuclear diameter (fine vertical line underneath the bars representing the barley chromosome arm). The positions of the telomere (grey vertical bar) and centromere (red vertical bar) are indicated by uppercase letters (C and T, respectively). Descriptive statistical data is shown on the right side.
(d) Diagram showing the proportion of cells carrying paired 7HL centromeres (green line) and paired 7HL telomeres (grey line) during different stages of prophase I. Initiation of pairing is marked by red circles in both cases.

chromosome segments, the larger proportion of the chromosome arm, which also carried the centromere-specific G + C FISH signal, maintained the condensed organisation observed in early leptotene (chromosome width: 0.7–1.81 μm), showing that decondensation of chromatin did not extend to the interstitial- and pericentromeric regions (Figure 3a–c). The decondensed subtelomeric region covered half (53.8%) of the total length of the chromosome arm measured in late leptotene (28.7 ± 10.1 μm; mean ± SD; $n = 27$), which corresponded to the length of the diameter of the nucleus (32.7 ± 10.0 μm; mean ± SD; $n = 27$) (Figure 3c). This indicated a chromosome arm elongation of 35% compared to early leptotene. The barley chromosome arms become synchronously decondensed along their entire length in early zygotene and reached their maximum prophase I length (62.02 ± 21.4 μm; mean ± SD; $n = 25$) (Figure 3a–c). The quasi-parallel organisation of the homologous chromosome arms was retained up to early zygotene, with the telomeres and the centromeres oriented at the two extremes of the nucleus.

Barley centromeres follow dynamics characteristic of the host genome

To reveal whether barley centromeres follow the activity of wheat chromosomes during the highly dynamic early stages of prophase I, we performed ImmunoFISH experiments, where we simultaneously applied barley centromere-specific G + C repeat sequence FISH with CENH3 immunolabelling to meiocytes ranging from leptotene to early-mid zygotene. CENH3 labelling showed all the active centromeres present, whereas the G + C DNA probe indicated the nuclear localisation of the barley centromere part of the translocation chromosome. The barley centromere-specific repeat overlapped with the CENH3 signal in all nuclei analysed ($n = 147$), indicating that the barley centromere loads centromere-specific histone protein in the wheat background and thus represents a functional centromere. In leptotene, when large, polarised centromere groups are formed in wheat (ranging from nine to 15 groups), the two homologous barley centromeres were observed to join different groups (Figure 4, top row). In early zygotene (Figure 4, middle row) and early-mid zygotene nuclei (Figure 4, lower row), the barley centromeres were still separated from one another but occupied smaller groups or were perceived individually, most likely as a result of the progressive dispersion of large centromere clusters. We measured the regions marked by the barley centromeric repeat DNA probe from leptotene to early-mid zygotene aiming to reveal whether they undergo reorganisation between leptotene and early zygotene, typical of wheat chromosomes (Sepsi et al., 2017). An elongation of the G + C signal was observed between the period of leptotene (number of nuclei = 15) and early zygotene (number of nuclei = 15)

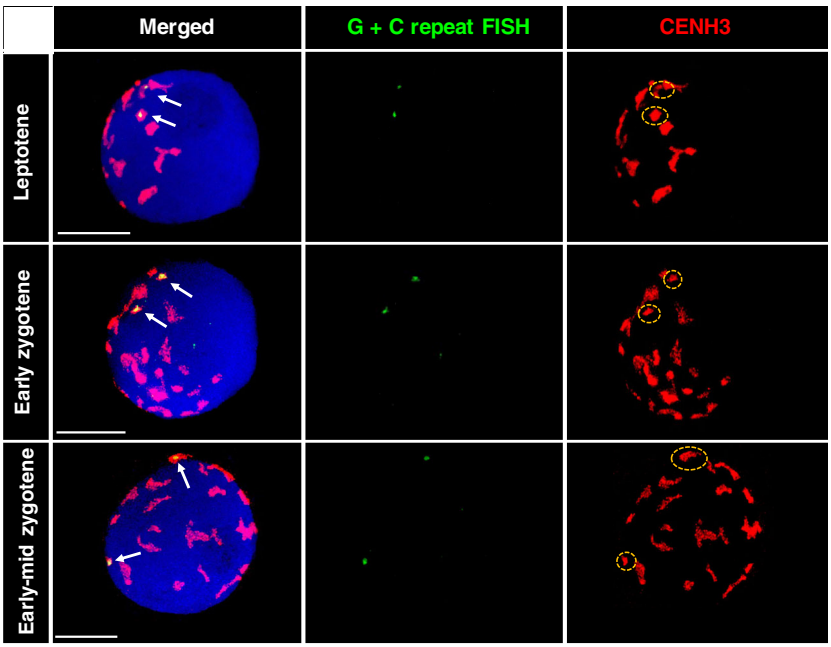

Figure 4. ImmunoFISH showing the relative position of homologous barley centromeres in nuclei of the 7BS.7HL Robertsonian translocation line at different substages of meiotic prophase I. Arrows in the merged image (left) indicate the barley centromeres marked by the G + C repeat sequences (FISH, Alexa 594, pseudo coloured in green) overlapping with the CENH3 (rabbit, detected by Alexa 488, green and pseudo coloured in red) signal, which visualise all active centromeres. The encircled (dashed yellow line) signal on the right shows the centromere group including the barley centromere. Meiotic nuclei were counterstained with DAPI. Scale bars = 5 μm.

(Figure S3), which did not increase further between early zygotene and early-mid zygotene (number of nuclei = 15). The barley centromere, representing half of the 7BS-7HL centromere, thus followed reorganisation dynamics similar to that of wheat chromosomes during the early stages of meiotic prophase I.

The progression of pairing between individual chromosome arms during zygotene

In a fraction of the analysed early zygotene nuclei (34%), homologous 7HL telomeres colocalised, whereas centromeres remained as two distinct foci at a considerable distance from one another (Figure 3a,d). Coincident with the appearance of telomere pairing, GISH showed the juxtaposition (the distance between the two chromosome threads was < 0.15 μm and thus they were perceived as one) of short chromosome segments located in the proximity of telomeres, indicating early events of chromosome synapsis within the subtelomeres (Figure 3a). Subtelomeres were defined as the chromosomal regions located near the telomeres that extended into the chromosome arms to the length observed to be decondensed at leptotene (17.91 ± 4.37 μm; mean ± SD) (Figure 3c). This region consisted of one-third of the total length of the fully decondensed chromosome arm as measured at zygotene (Figure 3c). These findings were in agreement with the results obtained from immunolabelling, which showed early traces of linear ZYP1. Progression of subtelomeric juxtaposition was evident in the majority of early-mid zygotene nuclei examined (n = 26). In some cases, juxtaposition was measured beyond the subtelomeres indicating early events of homologous interstitial chromosome contacts (Figure 3a). These colocalised 'juxtaposed interstitial segments' did not form a continuum with the juxtaposed subtelomeric regions; rather, a discontinuous interstitial juxtaposition became evident at a number of foci dispersed throughout the chromosome arms. This implied that homologous chromosome connections were regularly spaced by homologous non-colocalised 'interstitial chromatin alignments' varying in width between 0.2 and 7.3 μm (SD 0.7 μm; n = 26). The occurrence of the parallel alignments varied from cell to cell ranging from 5 to 23 with alignment lengths extending from 0.2 to 11.9 μm (SD 1.4 μm) (Figure 5). This was in line with our earlier studies showing multiple synapsis initiation sites within the chromosome arms and also with the immunolabelling results observed for the early-mid and mid-zygotene nuclei showing multiple synapsis initiation sites within the interstitial chromosome arms (see Figure 3a and Figure S2 and compare Figure 5a,b). Furthermore, *in situ* hybridisation showed that, although subtelomeric and interstitial regions were periodically united, the homologous barley centromeres marked by the G + C probe remained consistently at a considerable distance from one another, exhibiting a fork-like structure (Figure 3a,d). Importantly, centromeres no longer occupied a territory in the proximity of the nuclear periphery but were randomly located in the interior of the nucleus (Figure 3a,d). Their location varied from cell to cell, indicative of dynamic chromosome movement. Homologous centromere pairing was initially detected within a minority (14%) of the mid-zygotene nuclei (n = 70), whereas telomeres colocalised in the 94% of the pollen mother cells (Figure 3d) and juxtaposition of interstitial segments progressed into the pericentromeres (Figure 3a).

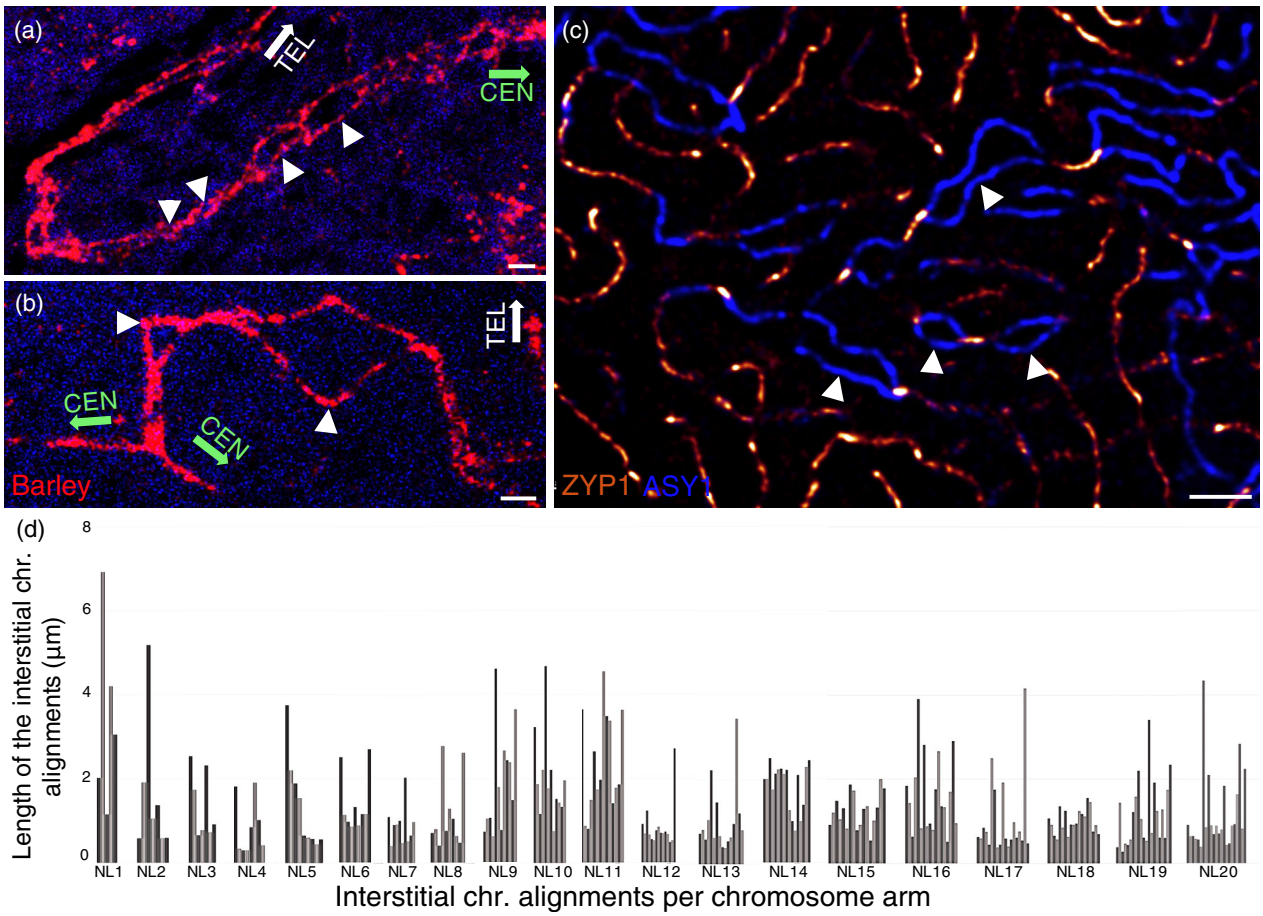

Figure 5. Patterns of homologous juxtaposition within the interstitial chromosome regions and the pericentromeres of the 7HL chromosome arm during zygotene.
(a, b) *In situ* hybridisation signal of the barley chromosome arm (in red) shows 'juxtaposed interstitial segments' disrupted by numerous non-juxtaposed 'interstitial chromatin alignments' (arrowheads). The orientation of the centromeres (CEN) and telomeres (TEL) are indicated by green and white arrows, respectively.
(c) ASY1 (blue threads) and ZYP1 (bright orange threads) immunolabelling shows similar patterns of interstitial synapsis interspersed by unsynapsed parallel axis alignments (arrowheads). Bars = 2 μm.
(d) Examples of the pattern and number of 'interstitial chromatin alignments' within the analysed barley chromosome arms, showing the length (*y*-axis) and number (*x*-axis) of parallel, non-juxtaposed chromosomal regions per chromosome arms. Groups represent data measured within one nucleus (Nl.) and thus a single pair of barley chromosome arms. Bars within one group from left to right represent measurements onwards the subtelomeres and progressing towards the centromeres.

Periodical juxtaposition connected a considerable amount of the chromosome arms at late-zygotene and the telomere bouquet began to disintegrate (Figure 3a,d). An increase in the frequency of centromere pairing was also observed (52% of nuclei displayed paired centromeres; $n = 58$). Full synapsis of the 7HL chromosome arms at pachytene coincided with an apparent arm shortening (52.0 ± 22.0 μm; mean ± SD; $n = 20$), indicative of chromatin condensation (Figure 3a,b).

Initiation of meiotic recombination in the 7BS.7HL line

Meiotic recombination initiation by SPO11-dependent DSBs can be detected cytologically with antibodies recognising the phosphorylation of the histone H2AX at the serine-139 residue, resulting in phospho histone H2AX ser139 (γH2AX) (Ku et al., 2020). To link SC axial element formation, centromere dynamics and ultimately chromosome arm morphogenesis with recombination initiation, we immunolabelled γH2AX foci together with ASY1 and CENH3 proteins in the pollen mother cell nuclei of the 7BS.7HL translocation line. Meiotic nuclei between the meiotic leptotene and zygotene stages exhibited numerous chromatin and axis associated γH2AX foci with considerable variation in fluorescence intensities (Figure 6a). We measured the relative fluorescence intensities of the immunolocalized γH2AX foci per individual leptotene and zygotene nuclei ($n = 23$) staged according to the ASY1/CENH3 signal. We observed a high relative fluorescence intensity γH2AX indicative of extensive DSB formation at leptotene ($n = 12$) when the homologous chromosome axes were continuous but still separated (Figure 6a,b). This was in agreement with previous studies reporting

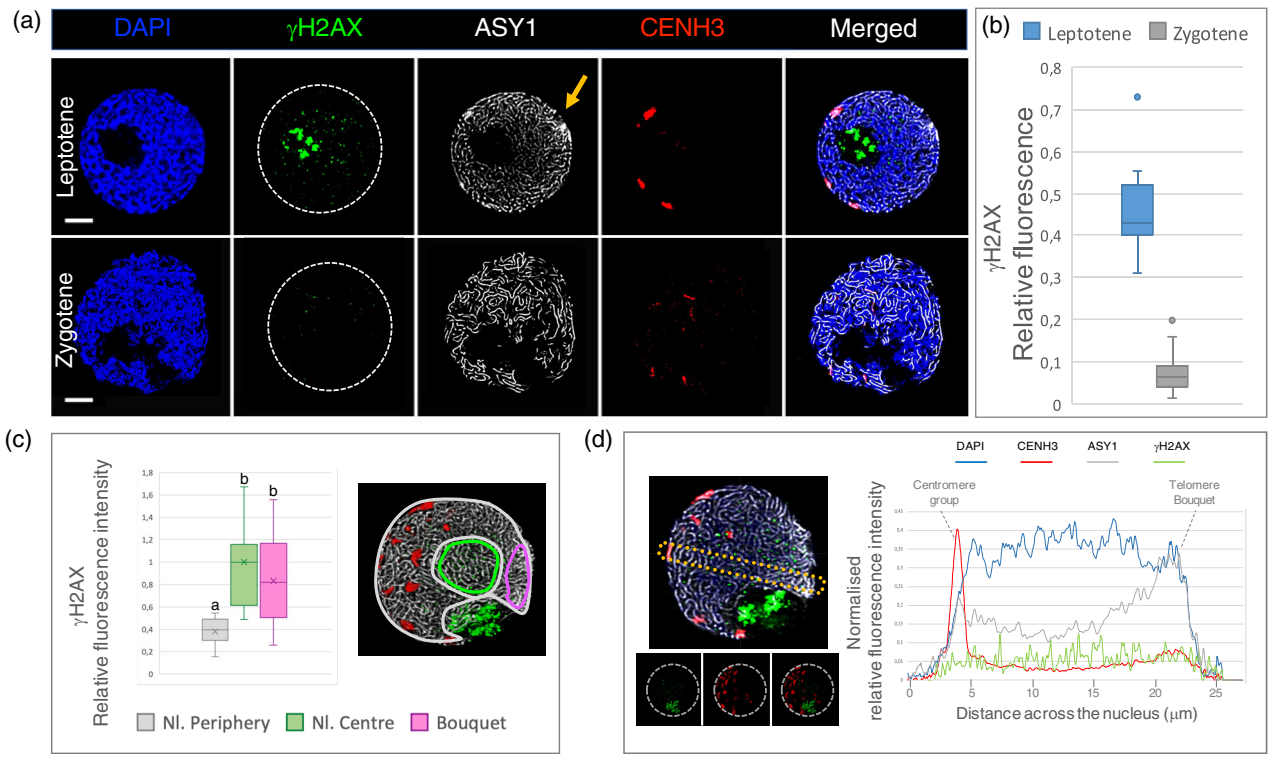

Figure 6. (a) Examples of microscopic images showing variations in the γH2AX levels between the leptotene and zygotene stages of the 7BS.7HL translocation line. γH2AX loci are labelled by an anti-γH2AX antibody (rabbit, detected by Alexa 488, green). For precise stage identification, the synaptonemal complex axial elements related protein ASY1 is shown using anti-ASY1 antibody (guineapig, detected by Alexa 647, pseudo coloured in grey) and CENH3 is sequentially labelled and visualized using anti-CENH3 antibody (rabbit, detected by Alexa 594, red). An orange arrow points to the telomere bouquet apparent by the concentrated ASY1 signal at leptotene.

(b) Relative fluorescence intensities of the γH2AX signals measured at the leptotene and zygotene stages in the 7BS.7HL translocation line. Significant differences were detected by Student's *t*-test ($P = 0.0005$).

(c) Spatial distribution of the γH2AX signal within the leptotene nuclei of the 7BS.7HL translocation line. Comparative analysis of relative fluorescence intensities of the nuclear periphery (grey colour, Nl. periphery), the nuclear centre (green colour, Nl. centre) and the nuclear volume including the telomere bouquet (magenta, bouquet). Measurements for each region of interest were carried out in three-dimensions (*z* direction, right) with LAS X software. Significantly lower relative fluorescence intensities were detected for the nuclear periphery than the nuclear centre. The telomere bouquet, although peripherally located, shows comparable relative fluorescence intensity to the nuclear centre (analysis of variance, d.f.1 = 2; d.f. 2 = 30; $F = 11.07$; $^{***}P = 2.51 \times 10^{-5}$). Lowercase letters (a, b) indicate significant differences (by Tukey's honestly significant *post hoc* test) between groups.

(d) Comparison between the γH2AX levels within the peripherally located centromeric regions, the chromatin located at the nuclear centre and the subtelomeric regions. Variations in relative fluorescence intensities of the γH2AX signal are shown with respect to DAPI (blue line), CENH3 (red line) and ASY1 (grey line) signals across a single focal point (frame) of a leptotene pollen mother cell nucleus. DAPI demarcates the area of the nucleus. The CENH3 signal shows characteristic peripheral centromere localisation (indicated by a dotted line, 'centromere group'), whereas the elevated ASY1 signal intensity at the opposite pole of the centromere indicates the location of the telomere bouquet (highlighted by a dotted line). The top image of the microscopic photograph represents an example of the region of interest (yellow dotted line) selected for the measurements. The bottom image aims to represent the decline of the γH2AX signal around the centromeres.

[Correction added on 06 August 2021, after first online publication: Part (d) of Figure 6 has been corrected in this version.]

recombination initiation in late G2-leptotene (Ku et al., 2020; Osman et al., 2021; Storlazzi et al., 2008). Zygotene nuclei ($n = 11$), characterised by partially juxtaposed chromosome axes, showed a substantial (85%) drop in the γH2AX relative fluorescence intensity (Figure 6a,b), denoting the initiation of DNA repair mechanisms as reported in other studies (Mahadevaiah et al., 2001; Su et al., 2017; Woglar and Villeneuve, 2018).

DSBs distribution is non-random within the nucleus

To understand the spatial distribution of DSBs inside individual leptotene nuclei, we quantified the relative fluorescence intensity of γH2AX foci at the nuclear periphery and at the centre. The nuclear periphery carried significantly lower γH2AX intensity levels (< 50%) compared to the nuclear centre (Figure 6c). One specific region of the nuclear periphery distinguished by a concentrated conical ASY1 signal, indicative of the telomere bouquet, carried a γH2AX immunosignal comparable to that observed for the centre of the nucleus (Figure 6c), indicating a higher DSB activity in the vicinity of the telomeres. This is in agreement with the subtelomeric initiation of the early DSBs in both wheat and barley (Higgins et al., 2014; Osman et al., 2021).

Although DSBs are formed at leptotene, the centromeres are also peripherally located, opposite the telomeric pole (Carlton and Cande, 2002; Wen et al., 2012). We therefore examined whether the crossover devoid centromeric and pericentromeric regions carry reduced levels of recombination initiations at leptotene, as indicated by the lower DSB signals measured at the nuclear periphery. By selecting single focal planes containing both peripherally located centromeres and a prominent telomere bouquet at the opposite side of the nuclear periphery, we specifically measured fluorescence intensities in two dimensions within the centromeres (n = 13), the nuclear centre and the telomeres. According to our measurements, significantly lower DSB levels were detected within the chromatin marked by CENH3 staining compared to the nuclear centre and the telomeres (Figure 6d), indicating that the core centromere somehow protected but did not completely inhibit DSB formation. Centromeres carried 25% lower γH2AX intensities than the nuclear centre and 50% lower intensities than telomeres confirming extensive DSB formation within the subtelomeric regions (Figure S4).

DISCUSSION

Understanding the mechanisms influencing the spatial distribution of early meiotic events is increasingly important in crops where specific allele combinations may determine the productivity of recent varieties (Lambing and Heckmann, 2018). The present study correlates chromatin dynamics with key steps of recombination and synapsis by assaying a single pair of homologous barley chromosome arms added to the wheat genome (Figure 7) in the form of a translocation (7BS.7HL translocation) at the same time as providing a precise prophase I timing. The stability of the barley chromosome arm in the 7BS.7HL line, leading to stable meiosis II and full fertility, shows that the meiotic morphogenesis of the barley chromosome is relevant to the understanding of chromosome behaviour in wheat. Additionally, we have demonstrated that the activity of the barley centromeres and their dynamics within the wheat nucleus followed a meiotic program characteristic of the host genome. This is in agreement with previous studies on wheat-rye introgression lines confirming that the pattern of chromatin remodelling of the alien (rye) chromosome at meiosis is directed by the host genetic background in which the chromosome is present (Naranjo, 2018).

Chromatin reorganisation precedes chromosome juxtaposition at the subtelomeres

We established a coherent chronology of chromosome arm pairing by correlating chromosome arm morphogenesis with the progression of synapsis and recombination. We showed that, in early leptotene, chromosome arms were condensed and organised into irregular globular subdomains with telomeres and centromeres pointing to opposite poles of the nucleus. This condensed early chromosome conformation and the bipolar orientation of telomeres versus centromeres was in agreement with several previous studies analysing chromatin dynamics in wheat-rye introgression lines (Corredor and Naranjo, 2007; Maestra et al., 2002; Martínez-Pérez et al., 1999; Mikhailova et al., 2001; Schwarzacher, 1997). We demonstrated that this condensed chromatin structure coincided with recombination initiation by numerous nucleus wide DSBs, whereas homologous chromosome arms were located at considerable distances from one another (Figure 7).

By late leptotene when chromosome axes were fully linear, without any sign of synapsis emerging from the prominent telomere bouquet, the homologous arms become partially and synchronously reorganised. Reorganisation explicitly involved the elongation of subtelomeric chromatin, which emerged from the fully formed telomere bouquet (Figure 7). The elongation of subtelomeric chromatin during the period of telomere bouquet formation has already been demonstrated as one of the earliest events of meiotic prophase I by *in situ* hybridisation on whole floret vibratome sections of a wheat-rye recombinant chromosome line carrying an interstitial rye chromosome segment. Prior telomere clustering wheat subtelomeric regions elongated and then both rye homologous segments elongated synchronously and intimately aligned (Prieto et al., 2004). The conformational change of the subtelomeric chromatin was found to be triggered by the mutual recognition of homologous chromosome partners, followed by their intimate alignment, indicating the important role of chromatin unpackaging in the homology recognition process (Colas et al., 2008).

The present study, based on the timeline set up by synaptonemal protein labelling, showed that, although both barley subtelomeres were included in the bouquet in late leptotene, homologous chromosome arms, including the subtelomeres, remained physically separated and localised at a considerable distance from one another. This shows that extensive presynaptic homologous coalignments, as observed in *Sordaria macrospora* (Storlazzi et al., 2010), are absent in large genome cereals. Short regions of chromosome axes coalign in wheat leptotene nuclei as well (Sepsi et al., 2018), although, as a result of the large genome and the multitude of chromosome threads, it cannot be determined whether these alignments involve homologous chromosomes. The present analysis suggests that leptotene axis alignments may occur between non-homologues or represent transient inter- or intra-chromosomal associations as indicated by the tight chromatin packaging within the interstitial and pericentromeric chromatin.

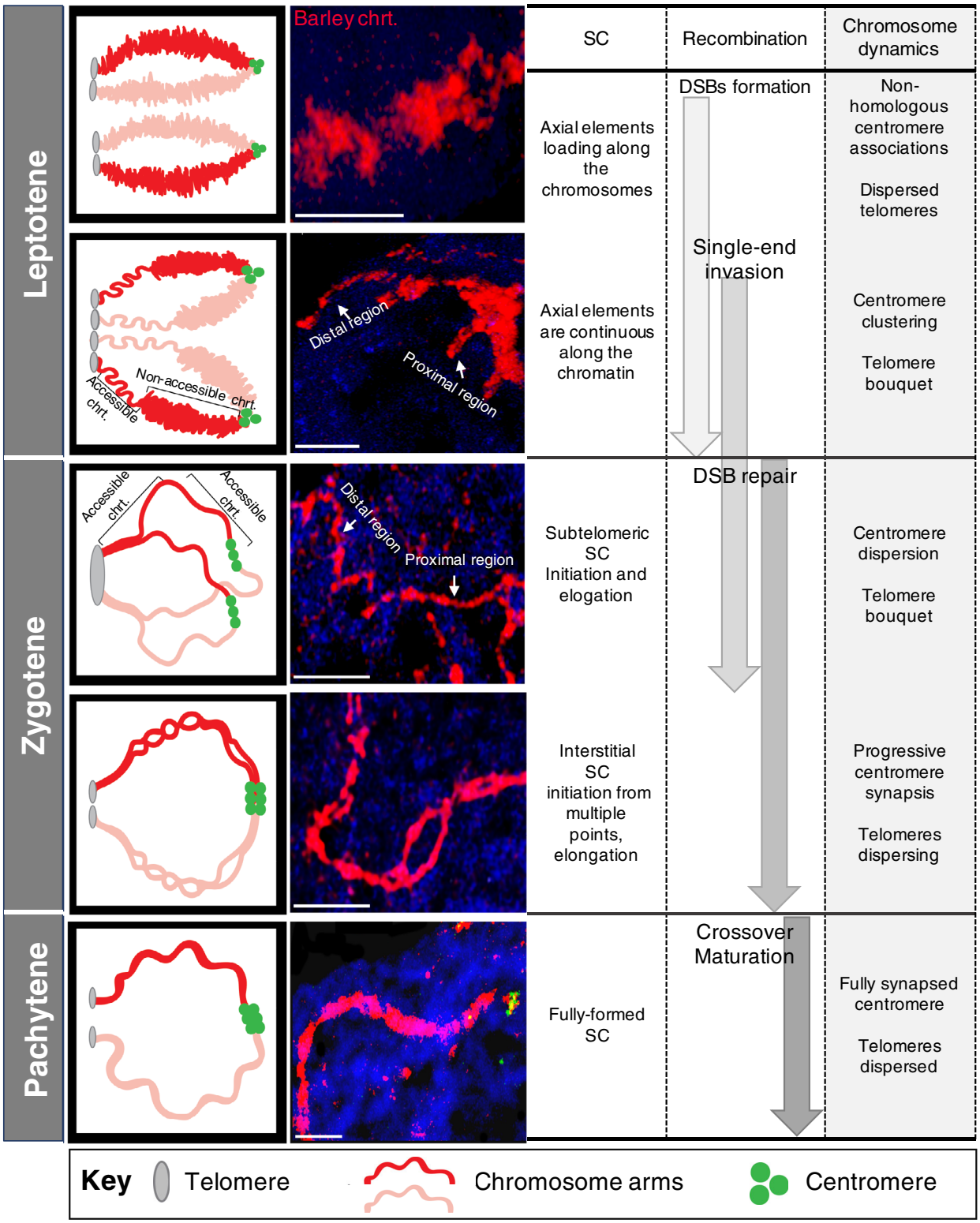

Figure 7. Chromatin dynamics, centromere and telomere associations during prophase I of meiosis. Left: Cartoon diagram of the chromatin morphogenesis and dynamics through the prophase I stages. Central panel: Microscopic images of single focal planes photographed within pollen mother cell nuclei of the 7BS.7HL wheat-barley line labelled with *in situ* hybridisation to detect the barley chromatin (Alexa Fluor 594, shown in red). Chrt., chromatin, Scale bars = 5 μm. Right: Chronology of synaptonemal complex (SC) development, recombination progression and chromosome dynamics during prophase I of meiosis (present study; Higgins et al., 2012; Osman et al., 2021; Sepsi et al., 2017).
[Correction added on 06 August 2021, after first online publication: The definition for Chromosome arms in the Key of Figure 7 has been corrected in this version.]

DSBs are predominant towards the centre of the nucleus and in the proximity of the telomere bouquet

Here, we showed that, although genome-wide DSBs are introduced at leptotene, the pericentromeric/interstitial chromatin remains initially enclosed in large globular domains, identical to their closed structure detected at the onset of meiotic prophase. Using quantitative image analysis, we detected a non-random distribution of DSBs inside the nucleus, where chromatin located at the nuclear periphery showed a lower DSB activity relative to the chromatin located at the nuclear centre. Subtelomeres, however, assembled into the telomere bouquet, showed an exception to this rule because they demonstrated DSB activity comparable to the nuclear centre. DSBs have been reported to be spatiotemporally confined to the subtelomeric regions prior to chromosome juxtaposition in wheat (Osman et al., 2021), barley (Higgins et al., 2012), zebrafish (*Danio rerio*) (Blokhina et al., 2019) and human males (Pratto et al., 2014) and have also been suggested to play a role in homology recognition and pairing.

When specifically assaying the core centromere of leptotene nuclei, we detected the lowest occurrence of recombination initiations, although centromeres were not completely devoid of DSBs. As expected, these events did not lead to crossovers, reflecting the local predominance of non-crossover repair. These results were in agreement with recent molecular work in wheat showing centromeric DSBs to be resolved as gene conversions representing non-reciprocal genetic exchanges (Gardiner et al., 2019). Examination of maize meiocytes showed that DSB formation at late leptotene coincides with a transient remodelling of axial elements as well, where a coiled axis morphology transitions to linear structures (Ku et al., 2020), suggesting a possible SPO11-1 dependent mechanism to orchestrate changes in axial element structures.

A significant variation in DSB distribution across the leptotene nucleus showed lower DSB activity for chromatin in proximity to the nuclear periphery, including the condensed centromeric chromatin. The subtelomeric regions showed an elevated DSB activity that coincided with the presynaptic chromatin remodelling into an open chromatin thread. The present study does not resolve whether the elevated DSB levels trigger chromatin remodelling at the subtelomeres or whether the open chromatin structure renders the subtelomeric region more prone to the DNA damage machinery. Chromatin remodelling is known as a key element of recombination patterning (Székvölgyi et al., 2015), although DNA damage itself can also affect chromatin organisation and mobility (Hauer and Gasser, 2017). An important question to consider is whether the compact chromatin structure together with the reduced DSB activity observed at the pericentromeres delays the recombination repair pathways and thus promotes non-crossover outcomes in the proximity of centromeres. This scenario is supported by evidence showing that the crossover/non-crossover decision is taken earlier in meiosis, possibly as early as DSB formation (Allers and Lichten, 2001; Bishop and Zickler, 2004). In line with this, a recent study in mice proposed that the fine scale chromatin structure and timing of DSBs influence the outcome of meiotic recombination. Earlier formed DSBs have been shown to occupy more open chromatin and be more prone to repair as crossovers than those that are formed later, suggesting that the crossover decision may need specific protein complexes that are absent at later stages (Chen et al., 2020).

Another element to be considered in terms of restricting crossover events within the centromeric/pericentromeric regions is the formation of early non-homologous centromere-centromere associations. They have been reported in cereal species (present study; Martinez-Perez et al., 2003; Phillips et al., 2012; Sepsi et al., 2017) and the model plant Arabidopsis (da Ines et al., 2012; Pradillo et al., 2014; Ronceret et al., 2009), although they appear in early meiotic prophase I of budding yeast (*Saccharomyces cerevisiae*) (Tsubouchi and Roeder, 2005) and *Drosophila melanogaster* (Kurdzo et al., 2017). Non-homologous centromere associations in wheat are consistent with earlier electron microscopy data on SC formation (Jenkins, 1983), revealing partner switches (homologous alignments interrupted by non-homologous pairing) within the interstitial chromosomal regions during zygotene. Non-homologous centromere interactions, thus ensuring spatial separation of the homologous centromeres, may to some extent prevent centromeric DSBs from being repaired via crossover pathways.

The present study suggests that the variation in chromatin packaging concentrates the whole chromosome recognition machinery to act initially at the subtelomeric regions. Homology testing and recognition promotes SC formation and progression of recombination repair mechanisms. Interstitial and pericentromeric regions may be masked by their globular, closed chromatin structure, implying a temporal shift in recognition, juxtaposition and initiation of repair, which results in the preference of the repair processes leading to non-crossovers.

Interstitial chromosome pairing progresses from multiple sites forming periodical juxtapositions interspersed with 'interstitial chromatin alignments'

The delayed remodelling of interstitial and pericentromeric chromatin compared to the subtelomeric regions (Figure 7) is in line with the temporal shift of the synapsis at the distal and proximal regions (Banerjee and Jones, 1999; Blokhina et al., 2019; Xiang et al., 2014). Initial chromatin juxtapositions occur between the subtelomeres in cereals. This process has been proposed to be mediated by the telomere bouquet and a telomere-led chromosome movement (Martinez-Garcia

et al., 2018; Sheehan and Pawlowski, 2009), which facilitates DSB-dependent homologous interactions specifically in the proximity of telomeres (Marshall and Fung, 2016). The specific composition of the subtelomeric DNA (Aguilar and Prieto, 2020; Calderón et al., 2014) may accelerate the recognition and juxtaposition process. As expected, homologous interstitial- and pericentromeric regions visualised in the present study showed multiple local juxtapositions that were interspersed by loose parallel chromosome arm alignments. These were in agreement with previous ultrastructural studies in wheat showing two bivalents connected by multiple short SC stretches located within the interstitial chromosomal regions (Holm, 1977, 1986; Jenkins, 1983). A similar pattern of SC development was reported in barley where subtelomeric synapsis was accompanied by multiple interstitial synaptic sites (Phillips et al., 2012).

The present study showed that apparition of intimate interstitial alignment and synapsis coincides with a considerable reduction in DSBs in zygotene, indicating initiation of crossover repair mechanisms.

The irregular, periodical pattern of interstitial juxtapositions suggested a progressive and random capture and connection of the homologous chromosome arms. During these dynamic juxtapositions, centromeres were released from the nuclear periphery. Their position varied greatly from cell to cell and their dynamics appeared to be solely limited by the progression of the pairing and attachment of their telomeres to the nuclear envelope. The direction of this random chromatin capture progressed from the subtelomeres towards the centromeres and reached the centromeres by late zygotene. Taken together, this reflects a coordinated highly dynamic pairing process, greatly influenced by the physical boundaries of the nuclear envelope and the association/release of the centromeres from the nuclear periphery, as well as the assumed, highly dynamic, telomere-led chromosome movement.

Here, we showed that changes in chromatin packaging are significant at the chromosome, chromosome arm and chromosome region level. Expanding knowledge on the coordination of chromatin dynamics with the fundamental processes of recombination and synapsis reveals chromosome pairing under the influence of a multitude of genetically/epigenetically defined physical factors, such as orientation, chromatin associations, nuclear envelope tethering, accessibility, proximity, tensions and movements. Spatiotemporal and functional relationships of these elements point to an evolutionary process that has shaped the chromatin context so that physical constraints acting on chromosomes are constantly accommodated during the highly complex homology recognition process to ensure a high-fidelity chromosome pairing and accurate transmission of the genome to the next generation. Further understanding of their role in meiotic processes may shed light on the complex mechanisms that result in the polarised distribution of the crossovers and thus contribute to crossover formation in chromosomal regions away from the telomeres.

EXPERIMENTAL PROCEDURES

Plant materials

The 7BS.7HL disomic translocation line used in the present study was obtained from a cross between the wheat/barley ('Asakazekomugi'/'Manas') 7H disomic addition line (carrying a pair of barley 7H chromosome in the normal wheat background, $2n = 44$, Molnár-Láng et al., 2012) and the Chinese Spring (CS) *ph* mutant line (carrying a mutation in the pairing homologous, *ph* gene; ref, Kansas State University, Manhattan, KS, USA; Genebank: TA 3809), which was performed to induce translocations between the wheat and barley chromosomes. Nine monosomic plants with a wheat-barley centric fusion chromosome were selected from 60 F_2 seeds by GISH. Following selfing of the F_2 generation, stable disomics were identified in the F_3.

For the fertility tests, the translocation plants and the parental wheat cultivars were grown in growth cabinets (Conviron PGR-15; Controlled Environments Ltd, Winnipeg, MB, Canada) in Martonvásár. Fifteen plants were randomly selected from CS wheat and the F_6 generation of the 7BS/7HL translocation line for fertility (seeds/floret) analysis.

Cytological procedures

Chromosome and nuclei preparation. Somatic chromosome spreads were developed as described by Kruppa et al. (2013). Meiotic tissue was fixed and prepared as described by Sepsi et al. (2018). In brief, the three anthers per florets (containing meiocytes in synchronised meiotic stages) (Bennett, 1971) were excised and divided as follows: two anthers were immediately transferred into fresh 4% paraformaldehyde to be processed for immunohistochemistry. The remaining (third) anther was placed into Carnoy fixative (ethanol: acetic acid, 3:1) and was later used for *in situ* hybridization. Position of the florets/spikelets/ear was recorded for each fixed anther to keep track of the progression of meiotic stages.

In situ hybridization. Total genomic DNA of 'Manas' barley, the barley barley-specific G + C-rich satellite sequences (Hudakova et al., 2001), the universal plant telomeric repeats (Schwarzacher and Heslop-Harrison, 1991) and the CRW (Li et al., 2013) were fluorescence labelled by nick translation (AF594 NT Labeling Kit, PP-305L-AF594; AF488 NT Labeling Kit, PP-305L-AF488; and AF647 NT Labeling Kit, PP-305L-AF647, respectively; Jena Bioscience, Jena, Germany) and hybridised together with unlabelled wheat genomic DNA used as blocking (at a ratio of 1:30) to somatic chromosome preparations of the wheat/barley translocation line. The CRW probe was prepared by polymerase chain reaction (PCR) amplification and labelled by nick translation (AF594 NT Labeling Kit, PP-305L-AF594). Hybridization procedures were carried out as described previously (Molnár-Láng et al., 2000) with minor modifications. The hybridization mixture contained 50% (v/v) deionised formamide (No. F9037; Sigma-Aldrich, St Louis, MO, USA), 10% (v/v) 20 × SSC solution (3 M NaCl; 0.3 M trisodium citrate dihydrate, pH 7.0), 1% (v/v) sodium dodecyl sulphate (10%, w/v; Sigma-Aldrich), 60 ng probe, supplemented with 2.4% (v/v) dextran sulphate (No. 67578; Sigma-Aldrich) in a final volume of 30 μl per slide. Slides were counterstaining in 18 μl of Vectashield Antifade Mounting Medium with DAPI (H-1200; Vector Laboratories, Burlingame, CA, USA).

For chromosome identification, GISH signals were washed off to perform a second, three-colour *in situ* hybridisation procedure using repetitive DNA probes of the Afa family (Nagaki et al., 1995), pSc119.2 (Bedbrook et al., 1980) and pTa71 (Gerlach and Bedbrook, 1979) repeats labelled by nick-translation with AF594 NT Labeling Kit, PP-305L-AF594; AF488 NT Labeling Kit, PP-305L-AF488; and AF647 NT Labeling Kit, PP-305L-AF647, respectively (Jena Bioscience).

Immunohistochemistry. Immunolabelling was carried out as described by Sepsi et al. (2017) with the following primary antibodies: anti-grassCENH3 (rabbit) (Sepsi et al., 2017), anti-AtASY1 (guinea pig) (Desjardins et al., 2020), anti-AtZYP1 (Osman et al., 2018) and anti-γH2AX (Rabbit; C15410219; Diagenode, Seraing, Belgium). To ensure that *in situ* hybridisation detects chromosome arm morphogenesis in the frame of an accurate meiotic staging and centromere dynamics, anti-CENH3, anti-ASY1 and anti-ZYP1 antibodies were applied to the anthers adjacent to anthers used for the *in situ* experiments. Recombination initiation by DSBs was detected using anti-γH2AX antibody. Preparations were incubated at 4°C overnight followed by an incubation of 3 h at 37°C. Slides were then washed twice in 1 × phosphate-buffered saline (137 mM NaCl, 2.7 mM KCl, 10 mM Na_2HPO_4 and 1.8 mM KH_2PO_4, pH 7.4) at room temperature for 5 min and incubated for 45 min at 37°C with anti-guinea-pig-Alexa 594, anti- rat-Alexa 488 and anti-rabbit-Alexa 647.

ImmunoFISH was carried out as described by Sepsi et al. (2018).

Molecular marker analysis—Genomic DNA was extracted from the wheat cultivar 'Chinese Spring', wheat/barley 7H addition line and the wheat/barley translocation line using Quick Gene-Mini80 (FujiFilm, Tokyo, Japan) with a Quick-Gene DNA tissue kit (FujiFilm). PCR reactions were carried out as described in Cseh et al., (2011) using Bmac0031 SSR and HvCSLF6 STS markers. PCR products were separated with a Fragment Analyzer™ Automated CE System equipped with a 96-Capillary Array Cartridge (Advanced Analytical Technologies, Ankeny, IA, USA). The results were interpreted using PROsize, version 2.0 (Advanced Analytical Technologies).

The deletion of the *Ph* gene from the 5BL chromosome arm was detected by the Xpsr574 STS marker as described by Roberts et al. (1999). Primers amplifying DNA fragments within the *ph1b* deletion can be used in a plus/minus PCR assay to detect lines carrying deletions in this region. The PCR products of 'Chinese Spring' *ph* mutant line, 'Asakazekomugi'/'Manas' 7H disomic addition line and the wheat/barley 7BS/7HL translocation line were separated using 2.2% SeaKem agarose gel (Cambrex Bio Science, East Rutherford, NJ, USA).

Confocal microscopy, image processing—Confocal microscopy was carried out using a TCS SP8 confocal laser-scanning microscope (Leica Microsystems GmbH, Wetzlar, Germany). Series of confocal images (*z* stacks) were acquired using a HC PL APO CS2 63×/1.40 oil immersion objective (Leica Microsystems GmbH). Size of confocal aperture was set to 0.65 Airy units. Image acquisition was carried out by bidirectional scanning along the *x*-axis, and images were averaged from three distinct image frames to reduce image noise. Fluorescence signals were detected using a hybrid detector set to photon counting mode for the accurate measurements. The fluorochromes used throughout the study were: DAPI (excited at 405 nm, detected from 410 to 450 nm), Alexa Fluor 488 (excited at 488 nm, detected from 490 to 520 nm), Alexa Fluor 594 (excited at 561 nm, detected from 565 to 620 nm) and Alexa Fluor 647 (excited at 633 nm, detected from 640 to 680 nm). Image stack deconvolution was performed using Huygens Essential, version 17.10 (Scientific Volume Imaging, Hilversum, The Netherlands).

Fluorescence signal intensities were measured on the collected image series (*z*-stacks) using Leica Advanced Fluorescence software, version 3.7.3.23245 (Leica Microsystems GmbH). Relative fluorescence intensities were determined by the quantifying functions 'Stack profile' and 'Line profile' of the software. Measurements were carried out on original, unprocessed (deconvolution, etc.) image series. All microscope settings (i.e. laser power, detector gain, detection spectra, etc.) were saved for each fluorescence labelled secondary antibody and kept the same throughout all the repetitions.

Statistical analysis

Fertility assay. To determine the possible differences between the fertility of CS (15 plants and 74 spikes) and the 7BS.7HL translocation line (15 plants and 73 spikes), we counted the relative fertility (number of seeds/florets/spikes) and computed the results using a *t*-test of independence. The assumption homogeneity of variances was tested and satisfied via Levene's *F*-test.

Chromosome arm length assay. Differences in the 7HL chromosome arm lengths within the defined meiotic phases (early leptotene, late leptotene, zygotene and pachytene) were measured using LAS X software (Leica Microsystems GmbH) on z-stacks obtained with confocal laser scanning microscopy. The measured lengths were analysed by one-way analysis of variance and classified using Tukey's B *post hoc* test.

Measured relative fluorescence intensity data were analysed by one-way analysis of variance and Tukey's B test, after the assumptions verified by the methods of d'Agostino (Tabachnick and Fidell, 2012). Statistical analyses were performed using SPSS, version 16.0 (SPSS Inc., Chicago, IL, USA).

Pairing between two loci (telomeres, centromeres and interstitial loci) was defined by measuring the interval in micrometre between them. Two homologous loci were counted as paired when the distance between them has fallen below a threshold of 0.2 μm (and thus were visually perceived as one).

ACKNOWLEDGEMENTS

The authors thank Dr John Bailey for revising the manuscript linguistically and we greatly appreciate the technical assistance of Ildikó Könyvesné-Lakner. We are grateful for Drs Márta Molnár-Láng and Gabriella Linc for providing support during the development of the plant material. AS acknowledges funding from the Hungarian Academy of Sciences (János Bolyai Research Scholarship), the Nemzeti Kutatási Fejlesztési és Innovációs Hivatal (NKFIH, proposal ID NKFI-FK-124266) and the ÚNKP-20-5-BME-286 New National Excellence Program (Ministry for Innovation and Technology, Hungary). AC acknowledges funding from the Nemzeti Kutatási Fejlesztési és Innovációs Hivatal (proposal ID NKFI-129221).

CONFLICT OF INTEREST

The authors declare no conflict of interest.

AUTHOR CONTRIBUTIONS

AS and AC designed the project and interpreted the results. ALT, AS and AC performed the research and

carried out data analysis. AF, EM and DM contributed to the confocal microscopy experiments, and performed the nuclear measurements and statistical analysis. AS and ALT wrote the paper.

DATA AVAILABILITY STATEMENT

All relevant data can be found within the manuscript and its supporting materials.

SUPPORTING INFORMATION

Additional Supporting Information may be found in the online version of this article.

Figure S1. Gel electrophoresis showing the deletion (CS*ph1b*) and presence (7H and 7BS.7HL lines) of the *Ph1* gene within the 5BL chromosome arm.

Figure S2. Analysis of the CENH3, ASY1 and ZYP1 immune signals during prophase I of the 7BS.7HL translocation line.

Figure S3. Length of the barley centromeres marked by the G + C repeat FISH signal during leptotene, early zygotene and early-mid zygotene

Figure S4. γH2AX relative fluorescence intensities measured at the centromere groups, the nuclear centre and the telomere bouquet.

REFERENCES

Aguilar, M. & Prieto, P. (2020) Sequence analysis of wheat subtelomeres reveals a high polymorphism among homoeologous chromosomes. *Plant Genome*, **13**, 1–22.

Allers, T. & Lichten, M. (2001) Differential timing and control of noncrossover and crossover recombination during meiosis. *Cell*, **106**, 47–57.

Armstrong, S.J., Caryl, A.P., Jones, G.H. & Franklin, F.C.H. (2002) Asy1, a protein required for meiotic chromosome synapsis, localizes to axis-associated chromatin in Arabidopsis and Brassica. *Journal of Cell Science*, **115**, 3645–3655.

Banerjee, R. & Jones, G.H. (1999) Initiation and progression of homologous chromosome synapsis in Crepis capillaris: variations on a theme. *Genome*, **42**, 867–873.

Barakate, A., Higgins, J.D., Vivera, S., Stephens, J., Perry, R.M., Ramsay, L. et al. (2014) The synaptonemal complex protein ZYP1 is required for imposition of meiotic crossovers in barley. *The Plant Cell*, **26**, 729–740.

Bass, H.W. (2003) Telomere dynamics unique to meiotic prophase: formation and significance of the bouquet. *Cellular and Molecular Life Sciences*, **60**, 2319–2324.

Bass, H.W., Marshall, W.F., Sedat, J.W., Agard, D.A. & Cande, W.Z. (1997) Telomeres cluster de novo before the initiation of synapsis: a three-dimensional spatial analysis of telomere positions before and during meiotic prophase. *Journal of Cell Biology*, **137**, 5–18.

Bedbrook, J.R., Jones, J., O'Dell, M., Thompson, R.D. & Flavell, R.B. (1980) A molecular description of telomeric heterochromatin in secale species. *Cell*, **19**, 545–560.

Bell, O., Tiwari, V.K., Thomä, N.H. & Schübeler, D. (2011) Determinants and dynamics of genome accessibility. *Nature Reviews Genetics*, **12**, 554–564.

Bennett, M.D. (1971) The duration of meiosis. *Proceedings of the Royal Society of London. Series B, Biological Sciences*, **178**, 277–299.

Bennett, M.D., Chapman, V. & Riley, R. (1971) The duration of meiosis in pollen mother cells of wheat, rye and Triticale. *Proceedings of the Royal Society of London. Series B, Biological Sciences*, **178**, 259–275.

Bennett, M.D., Finch, R.A., Smith, J.B. & Rao, M.K. (1973a) Time and duration of female meiosis in wheat, rye and barley. *Proceedings of the Royal Society of London. Series B, Biological Sciences*, **183**, 301–319.

Bennett, M.D., Rao, M.K., Smith, J.B. & Bayliss, M.W. (1973b) Cell development in the anther, the ovule, and the young seed of Triticum aestivum L. Var. Chinese Spring. *Philosophical Transactions of the Royal Society of London. Series B, Biological Sciences*, **266**, 39–81.

Bishop, D.K. & Zickler, D. (2004) Early decision; meiotic crossover interference prior to stable strand exchange and synapsis. *Cell*, **117**, 9–15.

Blokhina, Y.P., Nguyen, A.D., Draper, B.W. & Burgess, S.M. (2019). The telomere bouquet is a hub where meiotic double-strand breaks, synapsis, and stable homolog juxtaposition are coordinated in the zebrafish, Danio rerio. *PLoS Genetics*, **15**, e1007730.

Boden, S.A., Langridge, P., Spangenberg, G. & Able, J.A. (2009) TaASY1 promotes homologous chromosome interactions and is affected by deletion of Ph1. *The Plant Journal*, **57**, 487–497.

Calderón, M.D.C., Rey, M.-D., Cabrera, A. & Prieto, P. (2014) The subtelomeric region is important for chromosome recognition and pairing during meiosis. *Scientific Reports*, **4**, 6488.

Carlton, P.M. & Cande, W.Z. (2002) Telomeres act autonomously in maize to organize the meiotic bouquet from a semipolarized chromosome orientation. *Journal of Cell Biology*, **157**, 231–242.

Chacón, M.R., Delivani, P. & Tolić, I.M. (2016) Meiotic nuclear oscillations are necessary to avoid excessive chromosome associations. *Cell Reports*, **17**, 1632–1645.

Chambon, A., West, A., Vezon, D., Horlow, C., De Muyt, A., Chelysheva, L. *et al.* (2018) Identification of ASYNAPTIC4, a component of the meiotic chromosome axis. *Plant Physiology*, **178**, 233–246.

Chen, Y., Lyu, R., Rong, B., Zheng, Y., Lin, Z., Dai, R. *et al.* (2020) Refined spatial temporal epigenomic profiling reveals intrinsic connection between PRDM9-mediated H3K4me3 and the fate of double-stranded breaks. *Cell Research*, **30**, 256–268.

Colas, I., Darrier, B., Arrieta, M., Mittmann, S.U., Ramsay, L., Sourdille, P. *et al.* (2017) Observation of extensive chromosome axis remodeling during the "diffuse-phase" of meiosis in large genome cereals. *Frontiers in Plant Science*, **8**, 1–9.

Colas, I., Shaw, P., Prieto, P., Wanous, M., Spielmeyer, W., Mago, R. *et al.* (2008) Effective chromosome pairing requires chromatin remodeling at the onset of meiosis. *Proceedings of the National Academy of Sciences*, **105**, 6075–6080.

Corredor, E., Lukaszewski, A.J., Pachón, P., Allen, D.C. & Naranjo, T. (2007) Terminal regions of wheat chromosomes select their pairing partners in meiosis. *Genetics*, **177**, 699–706.

Corredor, E. & Naranjo, T. (2007) Effect of colchicine and telocentric chromosome conformation on centromere and telomere dynamics at meiotic prophase I in wheat-rye additions. *Chromosome Research*, **15**, 231–245.

Cseh, A., Kruppa, K., Molnár, I., Rakszegi, M., Doležel, J. & Molnár-Láng, M. (2011) Characterization of a new 4BS.7HL wheat-barley translocation line using GISH, FISH, and SSR markers and its effect on the β-glucan content of wheat. *Genome*, **54**, 795–804.

da Ines, O., Abe, K., Goubely, C., Gallego, M.E. & White, C.I. (2012) Differing requirements for RAD51 and DMC1 in meiotic pairing of centromeres and chromosome arms in Arabidopsis thaliana. *PLoS Genetics*, **8**, e1002636.

Desjardins, S.D., Ogle, D.E., Ayoub, M.A., Heckmann, S., Henderson, I.R., Edwards, K.J. *et al.* (2020) MutS homologue 4 and MutS homologue 5 maintain the obligate crossover in wheat despite stepwise gene loss following polyploidization. *Plant Physiology*, **183**, 1545–1558.

Gardiner, L.-J., Wingen, L.U., Bailey, P., Joynson, R., Brabbs, T., Wright, J. *et al.* (2019) Analysis of the recombination landscape of hexaploid bread wheat reveals genes controlling recombination and gene conversion frequency. *Genome Biology*, **20**, 69.

Gerlach, W.L. & Bedbrook, J.L. (1979) Cloning and characterization of ribosomal RNA genes from wheat and barley. *Nucleic Acids Research.*, **7**, 1869–1885.

Griffiths, S., Sharp, R., Foote, T.N., Bertin, I., Wanous, M., Reader, S. *et al.* (2006) Molecular characterization of Ph1 as a major chromosome pairing locus in polyploid wheat. *Nature*, **439**, 749–752.

Hauer, M.H. & Gasser, S.M. (2017) Chromatin and nucleosome dynamics in DNA damage and repair. *Genes & Development*, **31**, 2204–2221.

Heslop-Harrison, J.S.P. & Schwarzacher, T. (2011) Organisation of the plant genome in chromosomes. *The Plant Journal*, **66**, 18–33.

Higgins, J.D., Osman, K., Jones, G.H. & Franklin, F.C.H. (2014) Factors underlying restricted crossover localization in barley meiosis. *Annual Review of Genetics*, **48**, 29–47.

Higgins, J.D., Perry, R.M., Barakate, A., Ramsay, L., Waugh, R., Halpin, C. *et al.* (2012) Spatiotemporal asymmetry of the meiotic program underlies the predominantly distal distribution of meiotic crossovers in barley. *The Plant Cell*, **24**, 4096–4109.

Higgins, J.D., Sanchez-Moran, E., Armstrong, S.J., Jones, G.H. & Franklin, F.C.H. (2005) The Arabidopsis synaptonemal complex protein ZYP1 is required for chromosome synapsis and normal fidelity of crossing over. *Genes & Development*, **19**, 2488–2500.

Holm, P.B. (1977) Three-dimensional reconstruction of chromosome pairing during the zygotene stage of meiosis in Lilium longiflorum (thunb.). *Carlsberg Research Communications*, **42**, 103–151.

Holm, P.B. (1986) Chromosome pairing and chiasma formation in allohexaploid wheat, Triticum aestivum analyzed by spreading of meiotic nuclei. *Carlsberg Research Communications*, **51**, 239–294.

Hudakova, S., Michalek, W., Presting, G.G., ten Hoopen, R., dos Santos, K., Jasencakova, Z. *et al.* (2001) Sequence organization of barley centromeres. *Nucleic Acids Research*, **29**, 5029–5035.

Hunter, N. & Kleckner, N. (2001) The single-end invasion. *Cell*, **106**, 59–70.

Hurel, A., Phillips, D., Vrielynck, N., Mézard, C., Grelon, M. & Christophorou, N. (2018) A cytological approach to studying meiotic recombination and chromosome dynamics in Arabidopsis thaliana male meiocytes in three dimensions. *The Plant Journal*, **95**, 385–396.

Jenkins, G. (1983) Chromosome pairing in triticum aestivum cv. Chinese Spring. *Carlsberg Research Communications*, **48**, 255–283.

Jerković, I., Szabo, Q., Bantignies, F. & Cavalli, G. (2020) Higher-order chromosomal structures mediate genome function. *Journal of Molecular Biology*, **432**, 676–681.

Jordan, K.W., He, F., de Soto, M.F., Akhunova, A. & Akhunov, E. (2020) Differential chromatin accessibility landscape reveals structural and functional features of the allopolyploid wheat chromosomes. *Genome Biology*, **21**, 176.

Keeney, S., Giroux, C.N. & Kleckner, N. (1997) Meiosis-specific DNA double-strand breaks are catalyzed by Spo11, a member of a widely conserved protein family. *Cell*, **88**, 375–384.

Kruppa, K., Sepsi, A., Szakács, É., Röder, M. S. & Molnár-Láng, M. (2013) Characterization of a 5HS-7DS.7DL wheat-barley translocation line and physical mapping of the 7D chromosome using SSR markers. *Journal of Applied Genetics*, **54**, 251–258. https://link.springer.com/content/pdf/10.1007/s13353-013-0152-2.pdf

Ku, J.-C., Ronceret, A., Golubovskaya, I., Lee, D.H., Wang, C. & Timofejeva, L. *et al.* (2020) Dynamic localization of SPO11-1 and conformational changes of meiotic axial elements during recombination initiation of maize meiosis. *PLoS Genetics*, **16**, e1007881.

Kurdzo, E.L., Obeso, D., Chuong, H. & Dawson, D.S. (2017) Meiotic centromere coupling and pairing function by two separate mechanisms in Saccharomyces cerevisiae. *Genetics*, **205**, 657–671.

Lambing, C. & Heckmann, S. (2018) Tackling plant meiosis: from model research to crop improvement. *Frontiers in Plant Science*, **9**, 1–15.

Li, B., Choulet, F., Heng, Y., Hao, W., Paux, E., Liu, Z. *et al.* (2013) Wheat centromeric retrotransposons: the new ones take a major role in centromeric structure. *The Plant Journal*, **73**, 952–965.

Loidl, J. (2016) Conservation and variability of meiosis across the Eukaryotes. *Annual Review of Genetics*, **50**, 293–316.

Ma, Y., Kanakousaki, K. & Buttitta, L. (2015) How the cell cycle impacts chromatin architecture and influences cell fate. *Frontiers in Genetics*, **6**, 1–18.

Maestra, B., Hans de Jong, J., Shepherd, K. & Naranjo, T. (2002) Chromosome arrangement and behaviour of two rye homologous telosomes at the onset of meiosis in disomic wheat-5RL addition lines with and without the Ph1 locus. *Chromosome Research*, **10**, 655–667.

Mahadevaiah, S.K., Turner, J.M.A., Baudat, F., Rogakou, E.P., de Boer, P., Blanco-Rodríguez, J. *et al.* (2001) Recombinational DNA double-strand breaks in mice precede synapsis. *Nature Genetics*, **27**, 271–276.

Marshall, W.F. & Fung, J.C. (2016) Modeling meiotic chromosome pairing: nuclear envelope attachment, telomere-led active random motion, and anomalous diffusion. *Physical Biology*, **13**, 026003.

Martinez-Garcia, M., Schubert, V., Osman, K., Darbyshire, A., Sanchez-Moran, E. & Franklin, F.C.H. (2018) TOPII and chromosome movement help remove interlocks between entangled chromosomes during meiosis. *Journal of Cell Biology*, **217**, 4070–4079.

Martinez-Perez, E., Shaw, P., Aragon-Alcaide, L. & Moore, G. (2003) Chromosomes form into seven groups in hexaploid and tetraploid wheat as a prelude to meiosis. *The Plant Journal*, **36**, 21–29.

Martínez-Pérez, E., Shaw, P., Reader, S., Aragón-Alcaide, L., Miller, T. & Moore, G. (1999) Homologous chromosome pairing in wheat. *Journal of Cell Science*, **112**(Pt 11), 1761–1769.

Mercier, R., Mézard, C., Jenczewski, E., Macaisne, N. & Grelon, M. (2015) The molecular biology of meiosis in plants. *Annual Review of Plant Biology*, **66**, 297–327.

Mikhailova, E.I., Sosnikhina, S.P., Kirillova, G.A., Tikholiz, O.A., Smirnov, V.G., Jones, R.N. *et al.* (2001) Nuclear dispositions of subtelomeric and pericentromeric chromosomal domains during meiosis in asynaptic mutants of rye (Secale cereale L.). *Journal of Cell Science*, **114**, 1875–1882.

Molnár-Láng, M., Kruppa, K., Cseh, A., Bucsi, J. & Linc, G. (2012) Identification and phenotypic description of new wheat – six-rowed winter barley disomic additions. *Genome*, **55**, 302–311.

Molnár-Láng, M., Linc, G., Friebe, B. & Sutka, J. (2000) Detection of wheat-barley translocations by genomic in situ hybridization in derivatives of hybrids multiplied in vitro. *Euphytica*, **112**, 117–123. https://link.springer.com/content/pdf/10.1023/A:1003840200744.pdf

Murphy, S.P., Gumber, H.K., Mao, Y. & Bass, H.W. (2014) A dynamic meiotic SUN belt includes the zygotene-stage telomere bouquet and is disrupted in chromosome segregation mutants of maize (Zea mays L.). *Frontiers in Plant Science*, **5**, 314.

Nagaki, K., Tsujimoto, H., Isono, K. & Sasakuma, T. (1995) Molecular characterization of a tandem repeat, Afa family, and its distribution among Triticeae. *Genome*, **38**, 479–486.

Naranjo, T. (2018) Variable patterning of chromatin remodeling, telomere positioning, synapsis, and chiasma formation of individual rye chromosomes in meiosis of wheat-rye additions. *Frontiers in Plant Science*, **9**, 1–13.

Naranjo, T. & Corredor, E. (2004) Clustering of centromeres precedes bivalent chromosome pairing of polyploid wheats. *Trends in Plant Science*, **9**, 214–217.

Osman, K., Algopishi, U., Higgins, J.D., Henderson, I.R., Edwards, K.J., Franklin, F.C.H. *et al.* (2021) Distal bias of meiotic crossovers in hexaploid bread wheat reflects spatio-temporal asymmetry of the meiotic program. *Frontiers in Plant Science*, **12**, 1–20.

Osman, K., Sanchez-Moran, E., Higgins, J.D., Jones, G.H. & Franklin, F.C.H. (2006) Chromosome synapsis in Arabidopsis: analysis of the transverse filament protein ZYP1 reveals novel functions for the synaptonemal complex. *Chromosoma*, **115**, 212–219.

Osman, K., Yang, J., Roitinger, E., Lambing, C., Heckmann, S., Howell, E. *et al.* (2018) Affinity proteomics reveals extensive phosphorylation of the Brassica chromosome axis protein ASY1 and a network of associated proteins at prophase I of meiosis. *The Plant Journal*, **93**, 17–33.

Pecinka, A., Chevalier, C., Colas, I., Kalantidis, K., Varotto, S., Krugman, T. *et al.* (2020) Chromatin dynamics during interphase and cell division: similarities and differences between model and crop plants. *Journal of Experimental Botany*, **71**, 5205–5222.

Phillips, D., Nibau, C., Wnetrzak, J. & Jenkins, G. (2012). High resolution analysis of meiotic chromosome structure and behaviour in barley (Hordeum vulgare L.). *PLoS One*, **7**, e39539.

Pradillo, M., López, E., Linacero, R., Romero, C., Cuñado, N., Sánchez-Morán, E. *et al.* (2012) Together yes, but not coupled: new insights into the roles of RAD51 and DMC1 in plant meiotic recombination. *The Plant Journal*, **69**, 921–933.

Pradillo, M., Varas, J., Oliver, C. & Santos, J.L. (2014) On the role of AtDMC1, AtRAD51 and its paralogs during Arabidopsis meiosis. *Frontiers in Plant Science*, **5**, 23.

Pratto, F., Brick, K., Khil, P., Smagulova, F., Petukhova, G.V. & Camerini-Otero, R.D. (2014) DNA recombination. Recombination initiation maps of individual human genomes. *Science*, **346**, 1256442.

Prieto, P., Shaw, P. & Moore, G. (2004) Homologue recognition during meiosis is associated with a change in chromatin conformation. *Nature Cell Biology*, **6**, 906–908.

Roberts, M.A., Reader, S.M., Dalgliesh, C., Miller, T.E., Foote, T.N., Fish, L.J. *et al.* (1999) Induction and characterization of Ph1 wheat mutants. *Genetics*, **153**, 1909–1918.

Ronceret, A., Doutriaux, M., Golubovskaya, I.N. & Pawlowski, W.P. (2009) PHS1 regulates meiotic recombination and homologous chromosome pairing by controlling the transport of RAD50 to the nucleus. *Proceedings of the National Academy of Sciences of the United States of America*, **106**, 20121–20126.

Ronceret, A. & Pawlowski, W.P. (2010) Chromosome dynamics in meiotic prophase I in plants. *Cytogenetic and Genome Research*, **129**, 173–183.

Scherthan, H. (2001) A bouquet makes ends meet. *Nature Reviews Molecular Cell Biology*, **2**, 621–627. https://www.nature.com/articles/35085086

Schwarzacher, T. (1997) Three stages of meiotic homologous chromosome pairing in wheat: cognition, alignment and synapsis. *Sexual Plant Reproduction*, **10**, 324–331.

Schwarzacher, T. (2003) Meiosis, recombination and chromosomes: a review of gene isolation and fluorescent in situ hybridization data in plants. *Journal of Experimental Botany*, **54**, 11–23.

Schwarzacher, T. & Heslop-Harrison, J.S. (1991) In situ hybridization to plant telomeres using synthetic oligomers. *Genome*, **34**, 317–323.

Sepsi, A., Fábián, A., Jäger, K., Heslop-Harrison, J.S. & Schwarzacher, T. (2018) ImmunoFISH: simultaneous visualisation of proteins and DNA sequences gives insight into meiotic processes in nuclei of grasses. *Frontiers in Plant Science*, **9**, 1193.

Sepsi, A., Higgins, J.D., Heslop-Harrison, J.S.P. & Schwarzacher, T. (2017) CENH3 morphogenesis reveals dynamic centromere associations during synaptonemal complex formation and the progression through male meiosis in hexaploid wheat. *The Plant Journal*, **89**, 235–249.

Sepsi, A. & Schwarzacher, T. (2020) Chromosome–nuclear envelope tethering – a process that orchestrates homologue pairing during plant meiosis? *Journal of Cell Science*, **133**, jcs243667.

Sheehan, M.J. & Pawlowski, W.P. (2009) Live imaging of rapid chromosome movements in meiotic prophase I in maize. *Proceedings of the National Academy of Sciences of the United States of America*, **106**, 20989–20994.

Storlazzi, A., Gargano, S., Ruprich-Robert, G., Falque, M., David, M., Kleckner, N. *et al.* (2010) Recombination proteins mediate meiotic spatial chromosome organization and pairing. *Cell*, **141**, 94–106.

Storlazzi, A., Tesse, S., Ruprich-Robert, G., Gargano, S., Pöggeler, S., Kleckner, N. *et al.* (2008) Coupling meiotic chromosome axis integrity to recombination. *Genes and Development*, **22**, 796–809.

Su, H., Cheng, Z., Huang, J., Lin, J., Copenhaver, G.P., Ma, H. et al. (2017) Arabidopsis RAD51, RAD51C and XRCC3 proteins form a complex and facilitate RAD51 localization on chromosomes for meiotic recombination. *PLoS Genetics*, **13**, e1006827.

Székvölgyi, L., Ohta, K. & Nicolas, A. (2015) Initiation of meiotic homologous recombination: flexibility, impact of histone modifications, and chromatin remodeling. *Cold Spring Harbor Perspectives in Biology*, **7**, a016527.

Tabachnick, B.G. & Fidell, L.S. (2012) *Using multivariate statistics*, 6th edition. Boston, MA: Pearson.

Tiang, C.-L., He, Y. & Pawlowski, W.P. (2012) Chromosome organization and dynamics during interphase, mitosis, and meiosis in plants. *Plant Physiology*, **158**, 26–34.

Tsubouchi, T. & Roeder, G.S. (2005) A synaptonemal complex protein promotes homology-independent centromere coupling. *Science*, **308**, 870–873.

Türkösi, E., Darko, E., Rakszegi, M., Molnár, I., Molnár-Láng, M. & Cseh, A. (2018) Development of a new 7BS.7HL winter wheat-winter barley Robertsonian translocation line conferring increased salt tolerance and (1,3;1,4)-β-D-glucan content. *PLoS One*, **13**, e0206248.

Varas, J., Graumann, K., Osman, K., Pradillo, M., Evans, D.E., Santos, J.L. *et al.* (2015) Absence of SUN1 and SUN2 proteins in Arabidopsis thaliana leads to a delay in meiotic progression and defects in synapsis and recombination. *The Plant Journal*, **81**, 329–346.

Wen, R., Moore, G. & Shaw, P.J. (2012). Centromeres cluster de novo at the beginning of meiosis in Brachypodium distachyon. *PLoS One*, **7**, e44681.

Woglar, A. & Villeneuve, A.M. (2018) Dynamic architecture of DNA repair complexes and the synaptonemal complex at sites of meiotic recombination. *Cell*, **173**, 1678–1691.e16.

Xiang, Y., Miller, D.E., Ross, E.J., Sánchez Alvarado, A. & Hawley, R.S. (2014) Synaptonemal complex extension from clustered telomeres mediates full-length chromosome pairing in Schmidtea mediterranea. *Proceedings of the National Academy of Sciences of the United States of America*, **111**, E5159–E5168.

Zhang, L., Espagne, E., de Muyt, A., Zickler, D. & Kleckner, N.E. (2014) Interference-mediated synaptonemal complex formation with embedded crossover designation. *Proceedings of the National Academy of Sciences of the United States of America*, **111**, E5059–E5068.

Zickler, D. & Kleckner, N. (2015) Recombination, pairing, and synapsis of homologs during meiosis. *Cold Spring Harbor Perspectives in Biology*, **7** (1), a016626.